UCRL 34
Copy.

The Adjustment of the Magnetic Field in the University of California Synchrotron

By

Raymond David Robertson
B.S. (University of Colorado) 1942

THESIS

Submitted in partial satisfaction of the requirements for the degree of

MASTER OF SCIENCE

in

Electrical Engineering

in the

GRADUATE DIVISION

of the

UNIVERSITY OF CALIFORNIA

Approved:

.....

.....

.....

Committee in Charge

Deposited in the University Library.....

Date Librarian

DISCLAIMER

TABLE OF CONTENTS

LIST OF ILLUSTRATIONS

Figure

Figure

INTRODUCTION

The synchrotron[1,2,3] is a machine for accelerating electrons to very high energies at a nearly constant orbit radius. From the time the electron is injected until it reaches an energy of two million electron volts the machine operates as a betatron[4,5,6,7]. After this time a radio frequency voltage is applied to the special accelerating resonator and the action is that of a synchrotron proper.

In order to insure that the electrons describe the desired orbits it is essential that the conditions of the magnetic field be known and further, that some of them satisfy particular relations during operation.

Considerable effort was expended to develop equipment capable of giving the desired information quickly and accurately and to outline procedures for the application of the proper corrections.

Original investigations of the problem were made by Dr. Wilson Powell and Dr. Arnold Clark. Their results were extended and applied by Carroll Mills and H. F. Kaiser in conjunction with members of the Electrical and Mechanical Engineering Departments. The author was assigned to the project in February 1947. The background of the problem was obtained from consultations with Carroll Mills, who was then working on other projects. Later problems were discussed with Dr. Wilson Powell under whose direction all of the magnetic design work was carried out. During the succeeding months experimental work was done using model magnets and a correlated procedure for the adjustment outlined. Equipment designed prior to the author's assignment was modified to conform with these later experimental results and other necessary testing components and equipments were designed and built.

1,2,3,4,5,6,7. All numeral superscripts refer to the item numbers listed in the bibliography.

PHYSICAL DESCRIPTION

The University of California synchrotron installation consists of the magnet and vacuum chamber, vacuum pumps, ignitron pulsing circuits, capacitor bank, injector system, radio frequency system, and control desk. The physical layout is shown in Fig. 1. The magnet and vacuum chamber are shown in more detail in Fig. 2. The outside dimensions of the magnet are 92 inches wide, 98 inches high and 184 inches long and it is composed of 66 slabs of .014 in. laminated high silicon transformer grade steel, 18 flux bars of .002 in. laminated steel as shown in Fig. 3, and two annular pole face assemblies separated by two plastic rings which fit snugly against the sides of the pole tips. The vacuum chamber is a fused quartz donut of elliptical cross section with major and minor axes approximately 5 1/4 in. and 2 1/2 in. respectively. This chamber contains an electron gun for injecting the electrons, an r-f resonator section whereby the electrons are accelerated to their final energy, and a target for collecting the electrons. This paper describes the experiments done to measure the field in this region and the requirements for adjusting this field. The vacuum pump and various auxiliary equipment are located near the magnet. Figures 4 through 10 show some of the details of the system.

The magnet is flanked on two sides by a wall of concrete blocks four feet in thickness for protection of personnel against radiation during operation. The other two sides face on a hill and valley respectively and require no other protection. The ignitron pulsing circuit, the resonating capacitors, and the general control panel from which all operations are controlled are located outside the shielding.

The excitation of the magnet consists of one sixty cycle pulse of current or one thirty cycle pulse of current recurring at any desired rate up to about six per second. Fig. 12B shows the actual field variation with time. The entire wave except for the small sections in the center

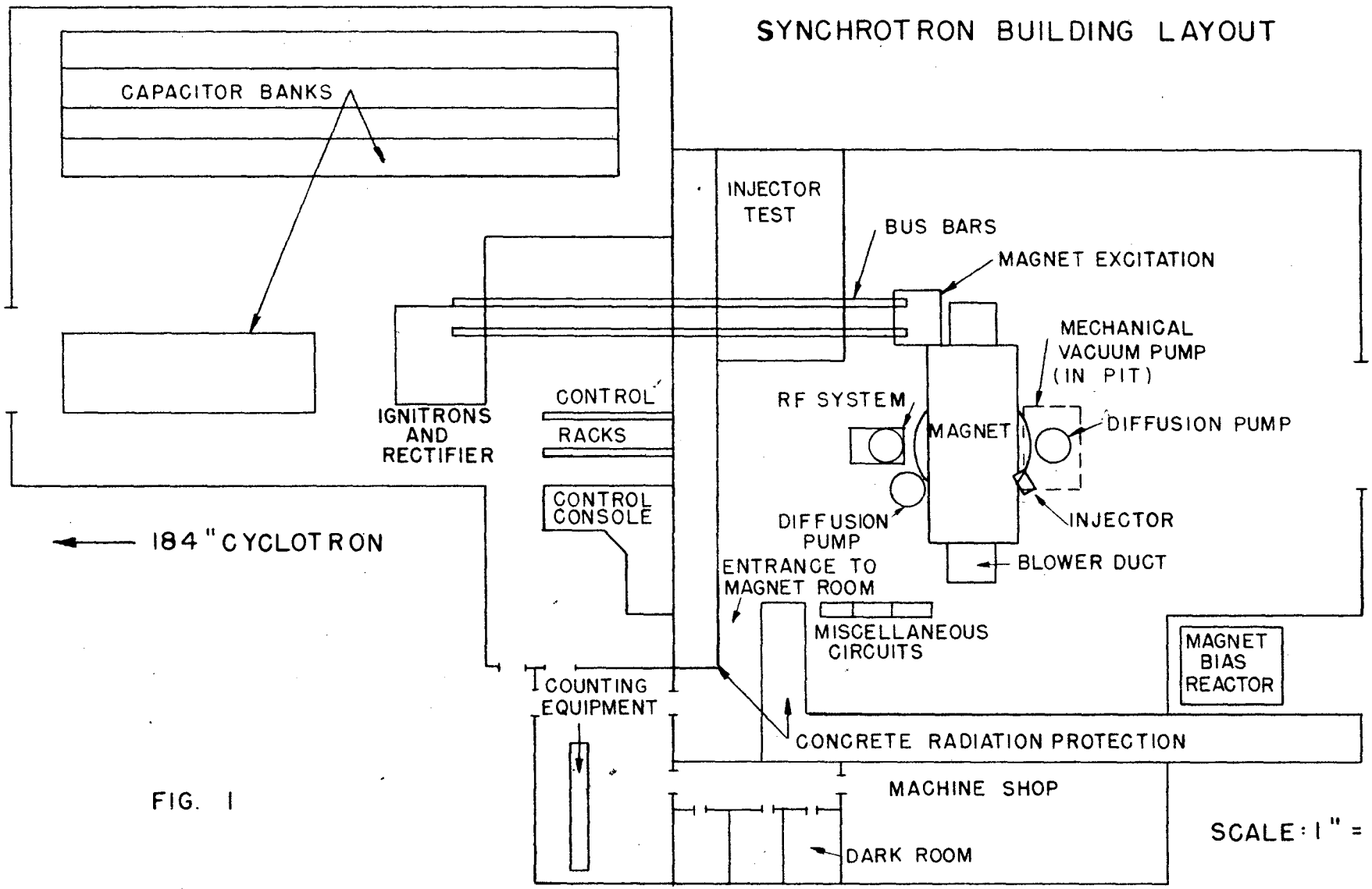
SYNCHROTRON BUILDING LAYOUT
CAPACITOR BANKS
INJECTOR TEST
BUS BARS
MAGNET EXCITATION
MECHANICAL VACUUM PUMP (IN PIT)
IGNITRONS AND RECTIFIER
CONTROL RACKS
RF SYSTEM
MAGNET
DIFFUSION PUMP
CONTROL CONSOLE
DIFFUSION PUMP
INJECTOR
184" CYCLOTRON
ENTRANCE TO MAGNET ROOM
BLOWER DUCT
MISCELLANEOUS CIRCUITS
MAGNET BIAS REACTOR
COUNTING EQUIPMENT
CONCRETE RADIATION PROTECTION
MACHINE SHOP
DARK ROOM
SCALE: 1" = 14'

FIG. 1

UNIVERSITY OF CALIFORNIA
SYNCHROTRON MAGNET

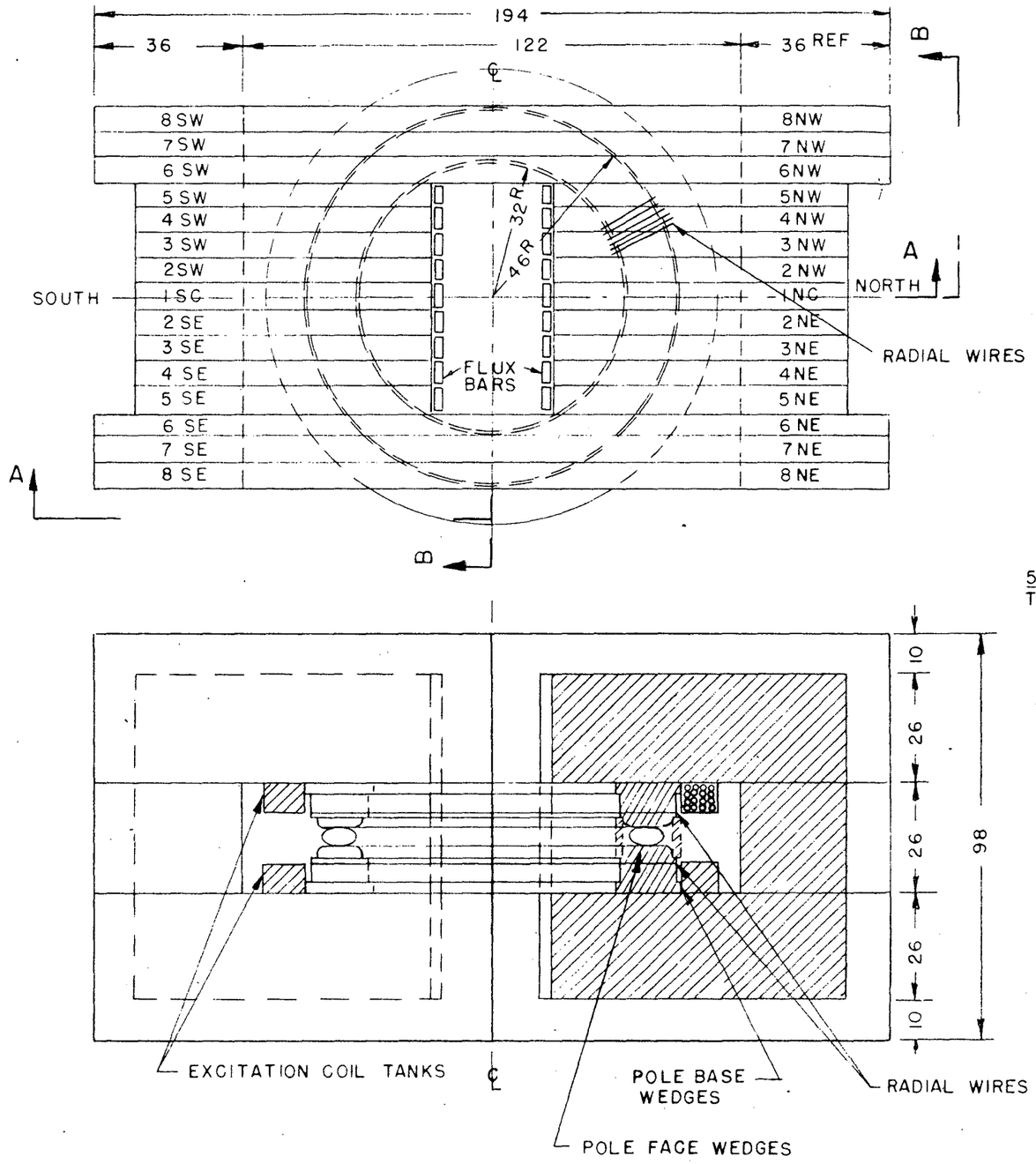

SECTION A – A

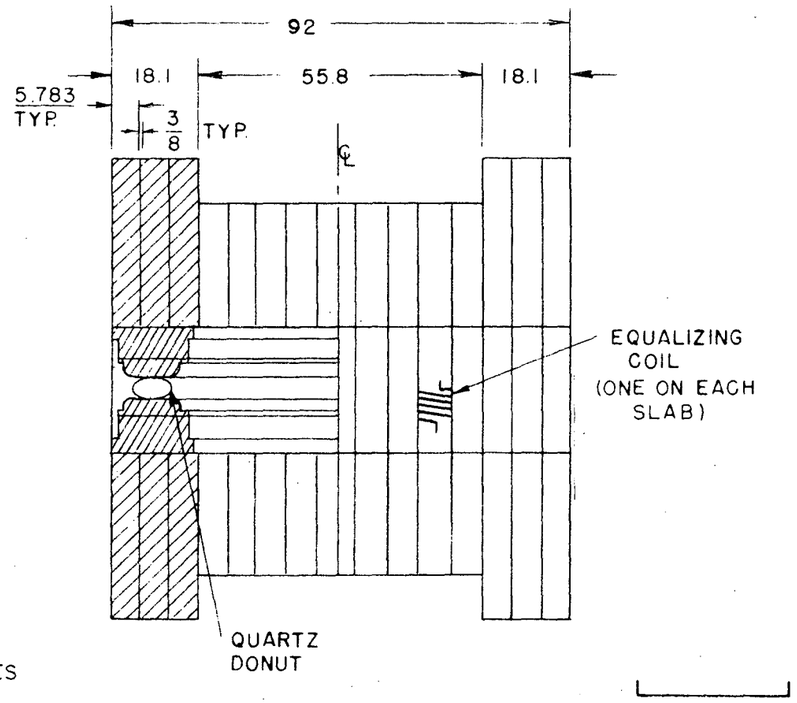

SECTION B – B

FIG. 2

13526-2

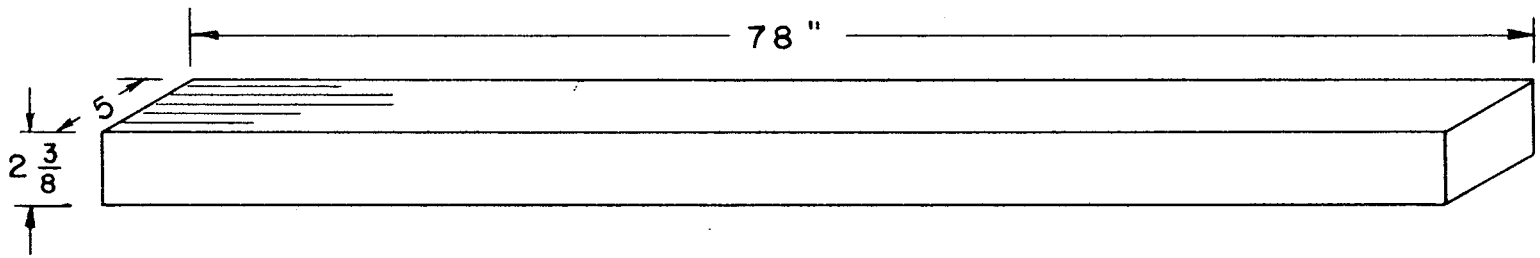

ARMCO THIN GAUGE ELECTRICAL STEEL.
960 LAMINATIONS .002" x 2 3/8" x 78"

FLUX BAR

FIG. 3

EAST SIDE OF MAGNET

FIG. 4

1. INJECTOR
2. DIFFUSION PUMP
3. LIQUID NITROGEN TRAP
4. Dr. E. McMILLAN WITH PHOTOMULTIPLIER BEAM MONITOR

OZ 408

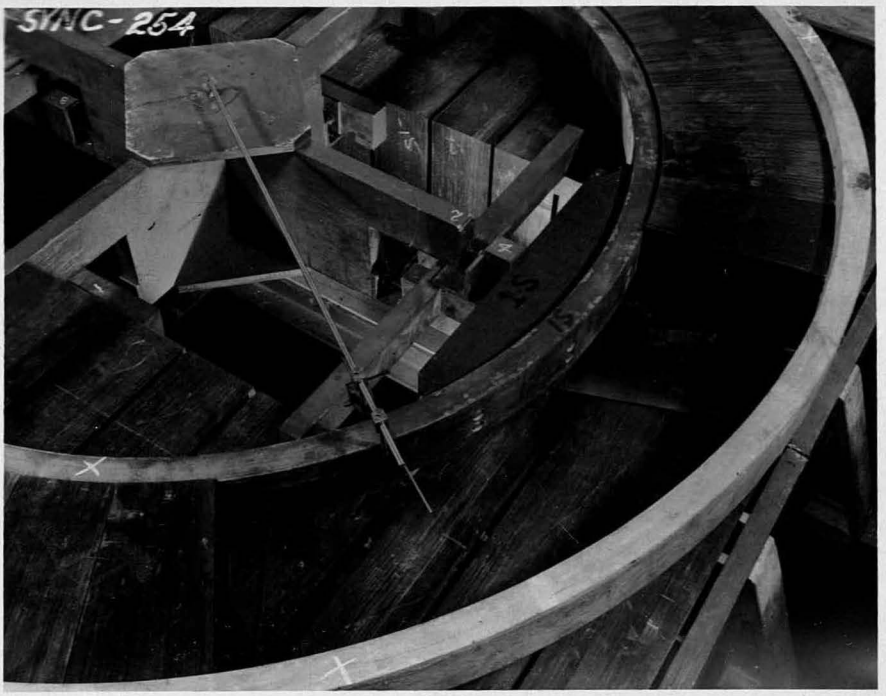

POLE BASE WEDGE CIRCLE
NEARLY COMPLETE

FIG. 5

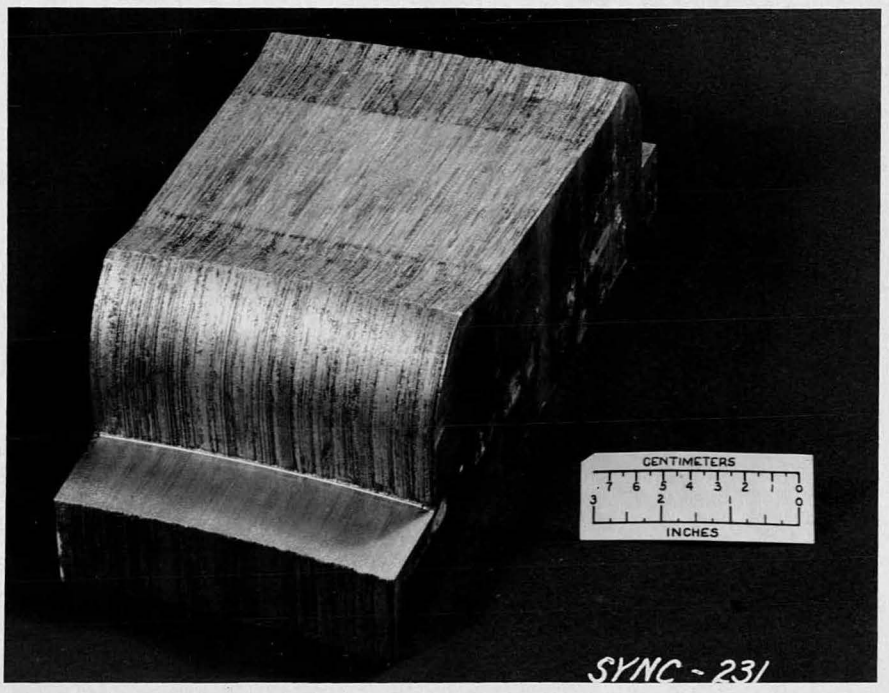

POLE FACE WEDGE

FIG. 6

QUARTZ DONUT

FIG. 7

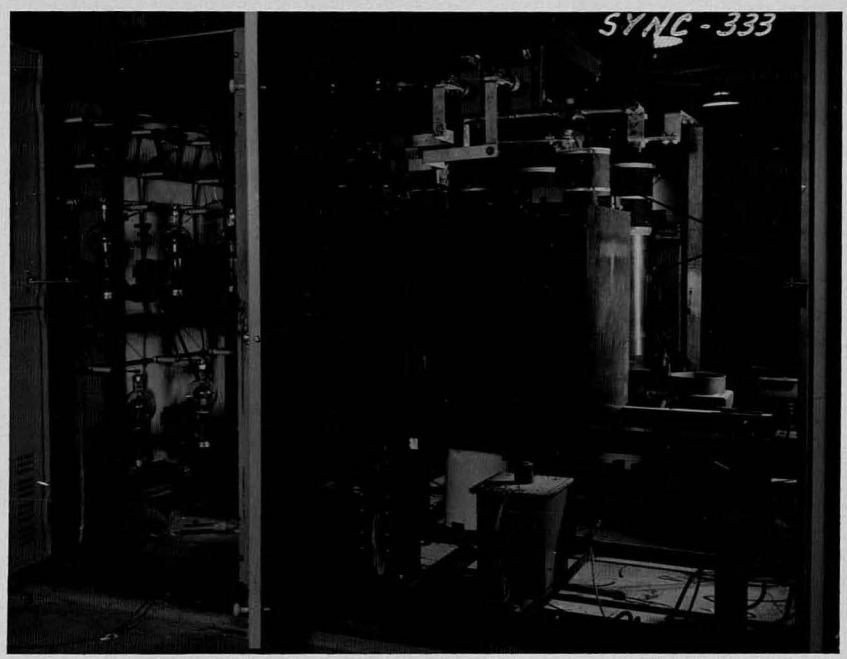

MAGNET EXCITATION CUBICLE

1. IGNITRONS
2. GRID FIRING BOX
3. RECTIFIER TUBES

FIG. 8

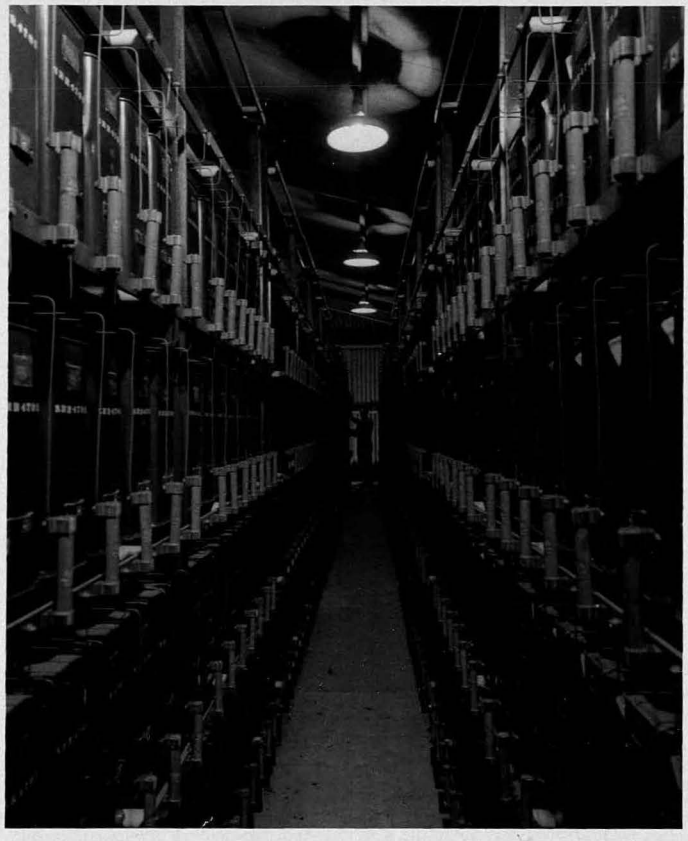

FIG. 9

ONE SECTION OF
CAPACITOR BANK

DR. McMILLAN AT THE CONTROL CONSOLE
FIG. 10

and at each end is approximately sixty cycles* and these small sections, which can be considered as portions of a twenty cycle wave of the same amplitude, are the periods during which the betatron acceleration conditions are satisfied. The pulses are formed by two ignitrons firing one-half cycle apart in time and connected as shown in Fig. 11. Each pair of ignitrons connects the magnet windings to the capacitor bank to form one-half of the excitation cycle. When the capacitor bank is charged to 16 Kv, a large current flows sinusoidally at the resonant frequency of the circuit in the direction permitted by the ignitron which is firing at that time. Fig. 12A shows the rate of change of field. The departure of the magnetic field from a true sine wave is due to the saturation of the flux bars and a resultant change in the effective inductance of the circuit during the period when they are not saturated.

Some of the characterisitcs of the system are:

Peak Voltage	16150 volts
Peak Current	4900 amperes
Inductance of magnet winding	8.75×10^{-3} henries
Capacitance	805 μ-farads
Power dissipated per cycle	6.28 k. w.
Total Peak Flux	2.68×10^{8} maxwells
Peak Induction Field	10000 gauss
Q	105
Electron Orbit radius	100 centimeters

To minimize the vibration due to the mechanical forces involved with such large rates of change of current, the magnet is mounted on a block of concrete which is insulated from the building foundation by shock absorbent pads.

A outaway view of the synchrotron is shown in Fig. 13.

*This paper will deal exclusively with the sixty cycle case.

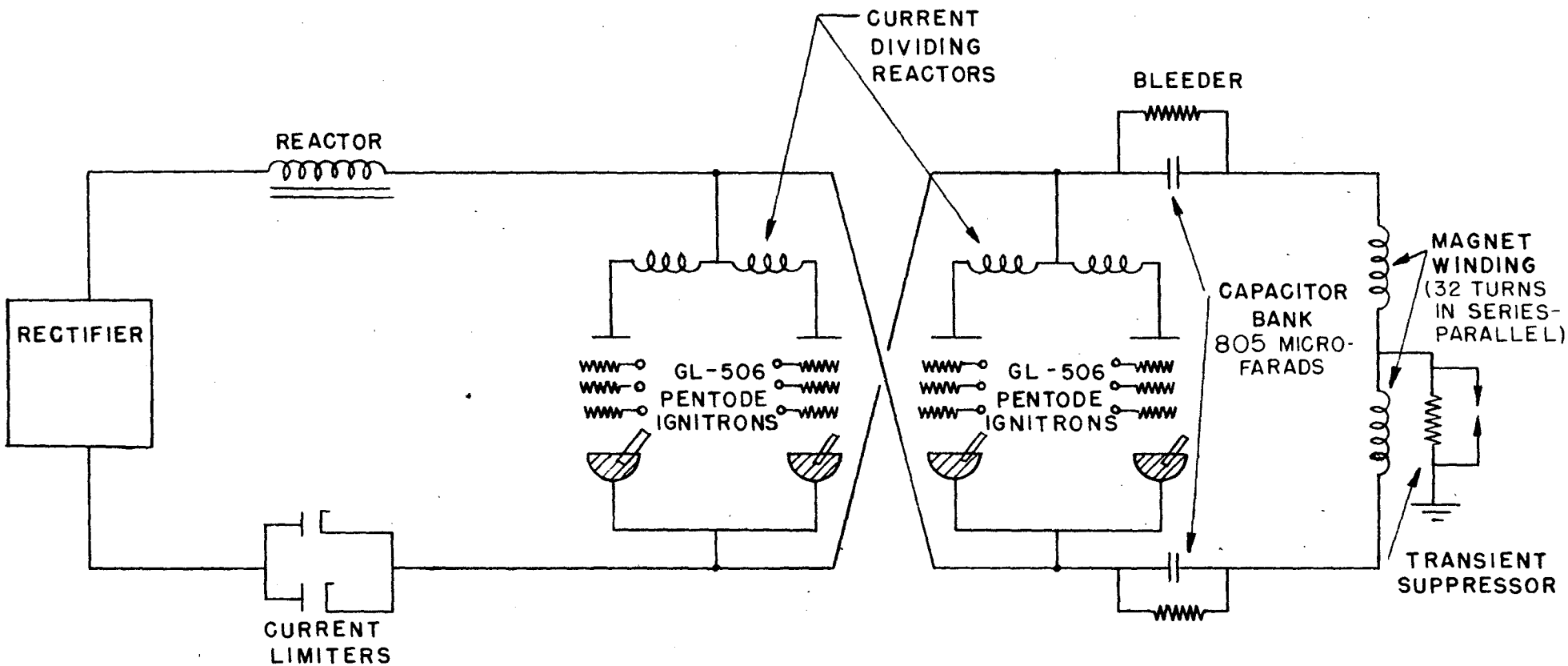

IGNITRON MAGNET PULSING CIRCUIT

FIG. II

13528-1

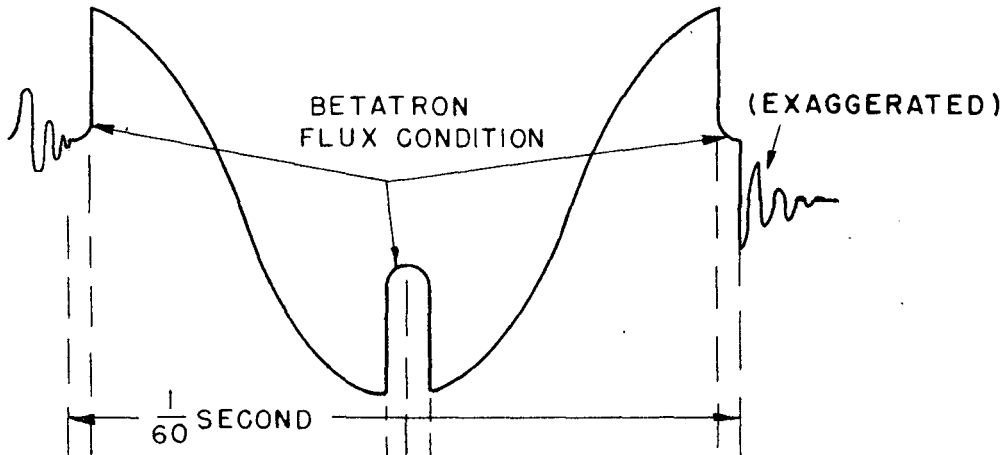

VOLTAGE WAVEFORM IN ACCELERATING GAP
WITH FLUX BARS IN POSITION

FIG. 12 A

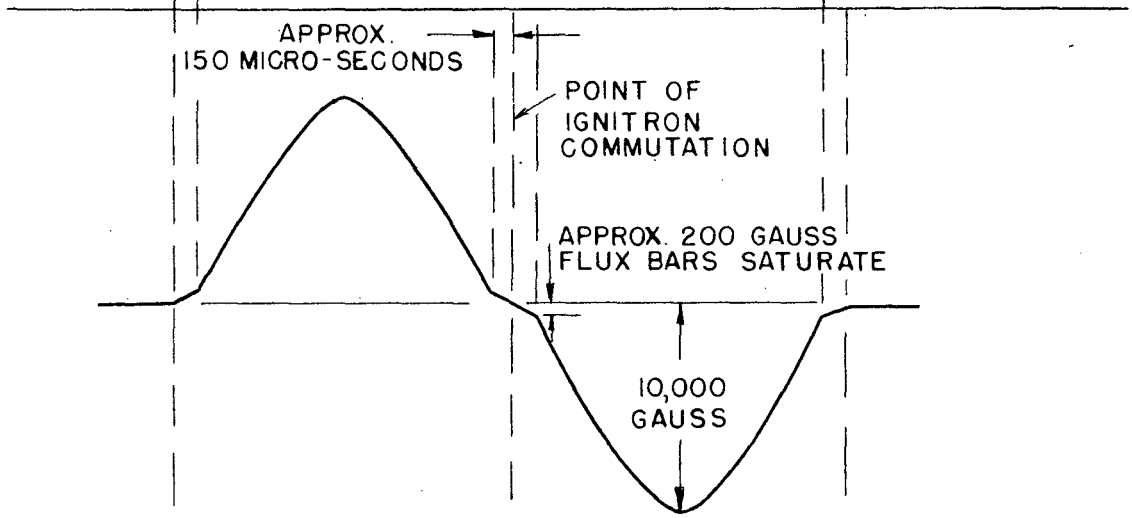

MAGNETIC FIELD VARIATION IN ACCELERATING GAP
WITH FLUX BARS IN POSITION

FIG. 12 B

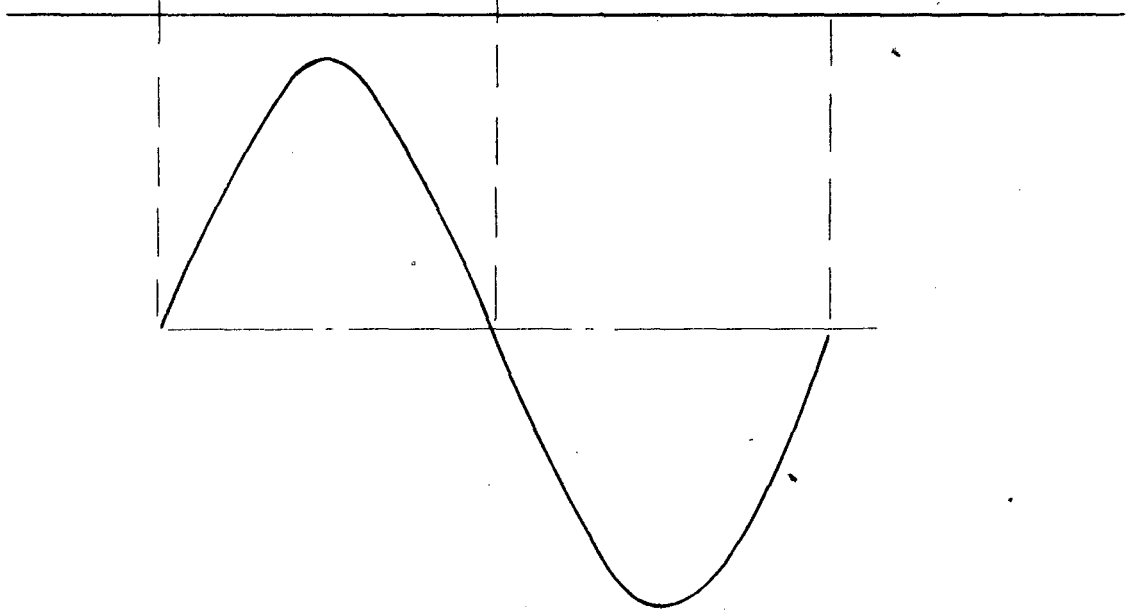

MAGNETIC FIELD VARIATION ACCELERATING GAP
WITH NO FLUX BARS IN POSITION

FIG. 12C

13529-1

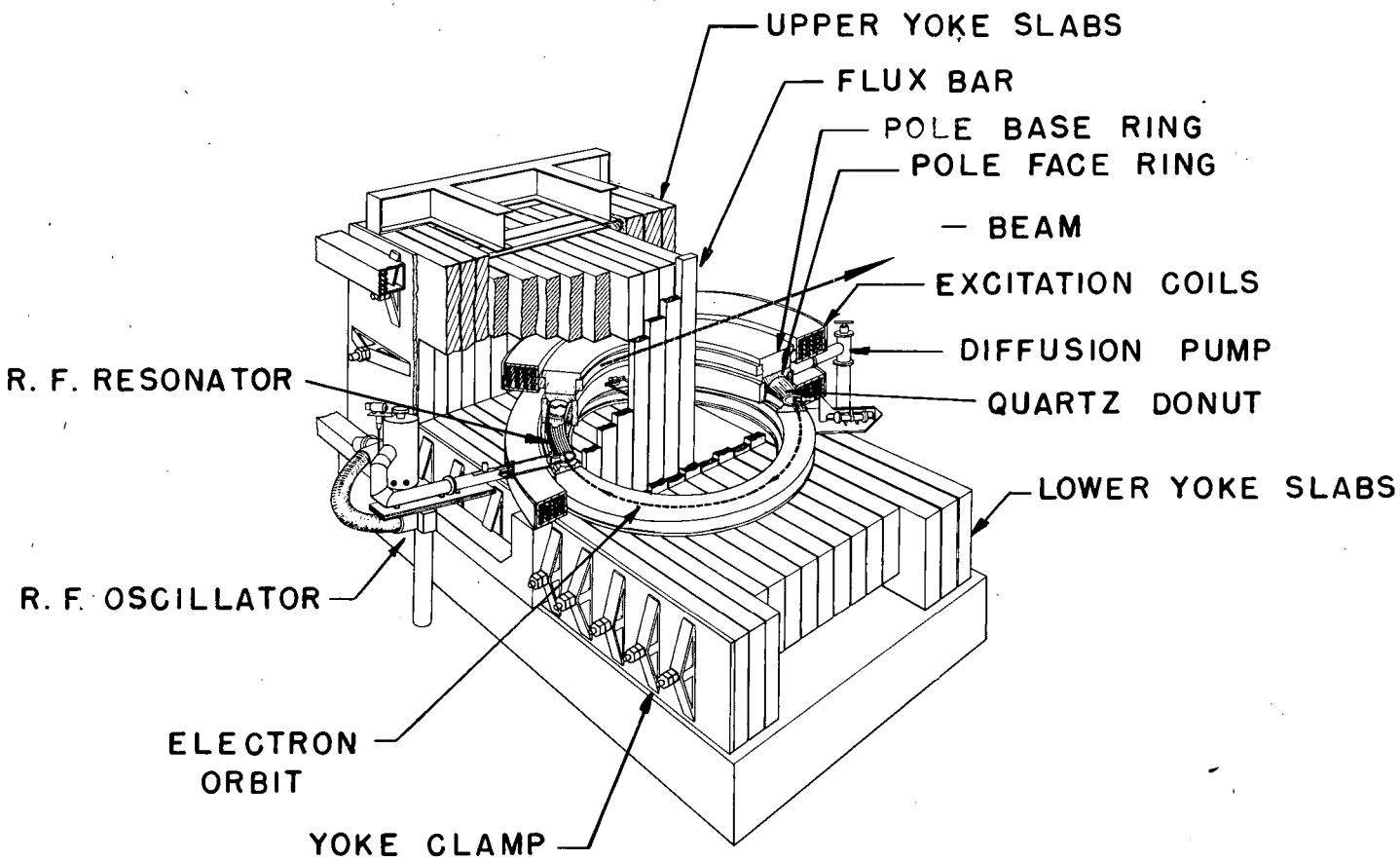

CUTAWAY VIEW OF SYNCHROTRON

FIG. 13

MAGNETIC FIELD REQUIREMENTS

A. General

No attempt will be made here to develop the theory of the synchrotron. References 2 and 3 elaborate these theoretical aspects. There are, however, a few basic requirements which must be met practically in order to insure efficient operation of the machine. The obvious first steps in the meeting of these requirements are careful design, meticulous manufacture of components and accurate physical positioning of these components. Beyond these precautions, corrective measures must be applied on the basis of measurements made after the assembly of the magnet.

B. Field Requirements

The required conditions for proper operation of the magnetic field are, in very general terms:

1. The magnetic field* must be identical within certain limits for all points at a given radius on the electron orbit at any given time during the operational cycle.

2. The variation of the magnetic field with radius must satisfy the theoretical relation, $B = B_0 (r_0/r)^n$, where B_0 is the field at the one meter orbit radius, r_0.

3. The theoretical relation $\dot{\phi}_0 = 2\pi r_0^2 \dot{B}_0$ must be satisfied during the betatron acceleration period, where $\dot{\phi}_0$ is the time rate of change of flux inside the orbit and $\dot{B}_0$ is the time rate of change of the field at the orbit radius, r_0.

Condition (1) requires that variations of the instantaneous magnitude of the field with azimuth at a constant radius be less than some

---

*It should be noted that in the literature the symbols B and H and the terms "field intensity" and "induction field" are used rather loosely when referring to phenomena in media where the permeability is unity, i.e., where the magnitudes of the two quantities are the same. In this paper the terms "induction field" and "field" will be used synonomously to refer to B and " field intensity" will refer to H.

maximum allowable value. These can be interpreted as phase variations as illustrated in Fig. 14. Examine two points at the same radii located in different portions of the magnet. Due to the lack of complete circular symmetry in the magnet the rates of change of field are different at these two points and due to eddy currents, remanence effects, and other non-uniformities in the magnetic structure the magnitudes of the fields at these points differ at any given time. This phase difference can be expressed as the difference in time for which the fields at the two points reach a certain value. From a knowledge of this time and the rates of change of field it is possible to determine the difference between the two fields at a given time. It was more convenient to measure the time phase difference than the actual difference in fields. In Fig. 14 we say that for a field of one gauss $\Delta t = t_B - t_A = 3$ micro-seconds is the phase error between points A and B. A graph of Δt vs. azimuthal position at a constant radius is called a phase plot. One 360 degree phase plot is the fundamental period of a recurrent waveform which may have an infinite number of harmonics.

The fundamental requirements given in the theory state only the effect of various harmonics in the phasing of the azimuthal field without establishing a definite criterion for the maximum allowable deviation from a perfectly phased field. The effect of the harmonics is given by:

$$\frac{x}{r_i} = \sum_{\ell=1}^{\infty} \frac{b_\ell}{\ell^2+n-1} \cos(\ell\theta + \ell a) \qquad (1)$$

where ℓ = the order of the harmonic (the fundamental is one revolution at the orbit radius).

$n = 2/3$, defined by $B/B_0 = (r_0/r)^n$.

x = the deviation from the instantaneous orbit.

r_i = the radius of the instantaneous orbit.

$b = \Delta B_\ell / B$, where ΔB_ℓ is the maximum deviation from the magnetic induction, B, of the ℓ^{th} harmonic.

θ = the angular distance around the orbit.

a = the phase of the ℓ^{th} harmonic.

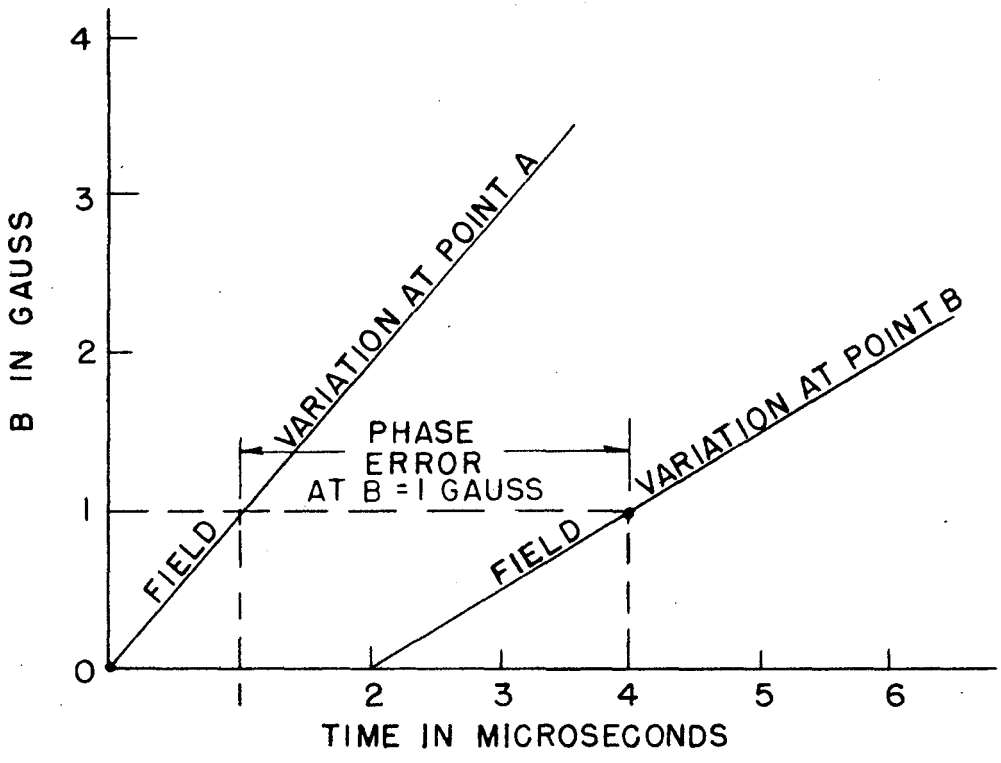

POINTS A AND B ARE TWO POINTS ON THE ORBIT AT THE SAME RADII.

ILLUSTRATION OF TIME PHASE VARIATION

FIG. 14

A criterion can be established by assuming the worst possible condition for addition of the harmonics in the above equation. This will occur when $\cos(\ell\theta + \ell\alpha) = 1$ for $0 < \ell < \infty$. It is not difficult to sum the right hand side of equation (1) by means of a Fourier analysis of the phase plot and the result obtained will be an upper bound of the actual perturbation. Only a few terms of the series need be taken since the factor $1/(\ell^2 + n-1)$ decreases quite rapidly. A maximum value of .05 was set for x/r_i which allowed a five centimeter variation in the orbit radius. An additional arbitrary limit of one gauss was set for the maximum variation, regardless of the order of the harmonic.

Phasing variations, when expressed in terms of time, are independent of the operating voltage to a first order of approximation in our machine. This was not expected to be the case because the phasing variations are made up of two components one of which is not theoretically a linear function of operating voltage. These two components are the variations due to eddy currents in the yoke and those due to remanence.

Appendix A outlines the mechanism of the eddy current effects and indicates that the change in field ΔB_e from such currents is proportional to $\dot{B}$, the rate of change of field.

$$\Delta B_e = K_1 \dot{B} \tag{2}$$

and the corresponding time:

$$\Delta t_e = \frac{\Delta B_e}{\dot{B}} = K_1 \frac{\dot{B}}{\dot{B}} = K_1 \tag{3}$$

Remanence is not theoretically a linear function of the operating voltage although it does depend on the magnetic history. As the iron tends toward saturation the remanent induction, B_r, increases less than proportionally. In general the remanent phase variation:

$$\Delta H_r = f(\phi \max) \tag{4}$$

$$\Delta t_r = \frac{\Delta H_r}{\dot{\phi}} = \frac{f(\phi \max)}{\dot{\phi}} \tag{5}$$

If $f(\phi \max) \approx K_2 \phi \max$

$$\Delta t_r = \frac{K_2 \phi \max}{\dot{\phi}} \tag{6}$$

For a particular geometry $\dot{\phi} = K_3 \phi \max$, then,

$$\Delta t_r = \frac{K_2 \phi \max}{K_3 \phi \max} = K_4 \tag{7}$$

For operation on the first half of the magnetic cycle in our machine the remanence is essentially zero. This is caused by the demagnetizing effect of a damped transient oscillation set up in a circuit consisting of the magnet inductance and stray capacity of the pulsing circuit at the cutoff time of the second ignitron.

For operation on the second half of the magnetic cycle the remanence, B_r, proves experimentally to be independent of the operating voltage over the range of usual operation.

This condition is indicated in Eqs. (6) and (7). Combining (3) and (7)

$$\Delta t = \Delta t_e + \Delta t_r = K_1 + K_4 = K_5 \tag{8}$$

Then, for a given geometry the phase lags expressed in terms of time are independent of the operating voltage. The rate of change of field at the time of injection, when the magnet is excited to its maximum field of 10,000 gauss, is 1.41 gauss per microsecond. Then, in terms of time, our arbitrary limit of one gauss corresponds to $\frac{\Delta B}{\dot{B}} = \frac{1}{1.41} = .7$ micro-second.

The relation set forth in section 2 above provides the desired magnetic focussing of the electron beam. Rearranging the equation:

$$Br^n = B_o r_o^n \tag{9}$$

Differentiating with respect to r:

$$r^n dB + Bnr^{n-1} dr = 0 \tag{10}$$

$$\frac{dB}{B} = -n \frac{dr}{r} \tag{11}$$

In incremental terms this becomes:

$$\frac{\Delta B}{B} = -n \frac{\Delta r}{r} \tag{12}$$

Interpretation of this equation shows that if the electron experiences

a change of radius Δr from some stable orbit radius r it will experience a change of field ΔB which tends to return it to the radius r. Quantitatively it is seen that again the most critical point for satisfying this equation is at the electron injection time. Choosing $\Delta r = 5$ cm. as a practical allowable variation from the stable orbit radius, $r = 100$ cm., and with $n = 2/3$* we get $\Delta B/B = .033$. At $B = 10000$ gauss $\Delta B = 330$ gauss. At the injection time when $B = 8$ gauss, $\Delta B = .26$ gauss. The latter requirement is quite stringent. Practically it was met by shaping the contour of the pole face to achieve the proper variation over about four inches in radius which was enough to more than include the predicted variations in orbital radius[3] during acceleration.

To achieve the third requirement listed above, (namely that $\dot{\phi}_o = 2\pi r_o^2 B_o$) a series of eighteen flux bars, one to bridge vertically between each pair of central slabs were installed as shown in Figs. 2, 3, and 13. These bars change the effective inductance of the magnet for a period of about 300 microseconds after the zero field point and at this time are allowed to saturate. They were designed to carry approximately two-thirds of the flux inside the orbit during the time before saturation. This satisfies the above equation for a long enough period of time to allow the electrons to reach 2 million electron volts. At this energy the electrons have reached 98 percent the velocity of light and the radio frequency acceleration is started.

The magnetic circuits form a rather complex system and their quantitative analysis was done largely through the use of models. In the following paragraphs a few qualitative analyses of the general operation of the magnetic structure will be made.

---

* n was chosen as 2/3 for theoretical reasons beyond the scope of this paper.

[3] See Bibliography

To explain the waveforms indicated in Fig. 12, consider the total magnetic flux, ϕ_T as given by:*

$$\phi_T = \phi_g + \phi_f = MMF_{AB}\left[\frac{1}{\mathcal{R}_g} + \frac{1}{\mathcal{R}_f}\right] \tag{13}$$

and its time rate of change:

$$\dot{\phi}_T = \dot{\phi}_g + \dot{\phi}_f \tag{14}$$

where ϕ_g = accelerating gap flux

ϕ_f = flux bar flux

$\mathcal{R}_g$ = reluctance of the accelerating gap circuit

$\mathcal{R}_f$ = reluctance of the flux bar circuit

The variational inductance of the circuit is given by:

$$L = K\frac{d\phi_T}{dI} = K\frac{\frac{d\phi_T}{dt}}{\frac{dI}{dt}} = K\frac{\dot{\phi}_T}{\dot{I}} \tag{15}$$

where I = the excitation current

From this point on all L's will refer to variational inductance. The circuit will have some value of inductance, L_B, during the betatron period when the flux bars are not saturated, and after the time when they saturate it will have some other value of inductance, L_S, for the synchrotron portion of the accelerating cycle. This is a result of the decrease in $\dot{\phi}_T$ which is due to the increase of the flux bar circuit reluctance, $\mathcal{R}_f$, at the time of saturation of the flux bars. (This change is not instantaneous as the flux bars do not saturate instantaneously.) After the flux bars saturate, equations (13) and (14) become:

$$\phi_T = \phi_g + \text{const} \tag{16}$$

$$\dot{\phi}_T = \dot{\phi}_g \tag{17}$$

Because the system is resonant a change in L is accompanied by a change in frequency and a proportional change in $\dot{I}$. It is seen from equation (15) that for a given L a change in $\dot{I}$ occasions a change in $\dot{\phi}_T$. In our system there is a change in both L and $\dot{I}$. In more quantitative terms, the constants of the circuit are such that:

$$L_B = 3\,L_S \tag{18}$$

*All subscripts refer to Fig. 15.

The currents corresponding to these inductances will be:

$$\dot{I}_B = \frac{\dot{I}_S}{3} \tag{19}$$

and the rates of change of flux will be:

$$\dot{\phi}_{TB} = \dot{\phi}_{TS} \tag{20}$$

Equation (19) indicates that the rate of change of current during the betatron acceleration period will be one-third that of the synchrotron acceleration period. This same relation exists between the rate of change of field in the gap during the two periods. This is shown in Fig. 12B. Fig. 12A is the differential of 12B and is the waveform obtained across the terminals of a coil placed in the field. Mathematically it is expressed by the equation, $E = -A\frac{dB}{dt}$. Equation (20) is a result of the relation, $E = K\dot{\phi}_T$, where E is the capacitor voltage which cannot change instantaneously.

There are two different types of magnetic circuit, one in which a flux bar directly shunts a top and bottom slab and the other in which there is no flux bar. This assymmetry, shown in Fig. 2, results in a rate of change of field which is non-uniform with azimuth. Slab numbers 1 through 5 are of the first type and numbers 6 through 8 are of the second type. Each circuit is actually slightly different because of the circular pole face geometry, but for purposes of explanation they will be treated only by type. In the analysis of the idealized magnetic circuits, their equivalent electrical circuits shown in Figs. 15 and 16 will be utilized. The accelerating gap will be treated as a uniform air gap and approximate values assigned to all other air gaps for ease of computation. A further approximation neglects the fringing flux and the reluctance of the iron. The use of the equivalent circuit presumes an analogy between the equations:

$$MMF = \phi R \tag{21}$$

and

$$E = IR \tag{22}$$

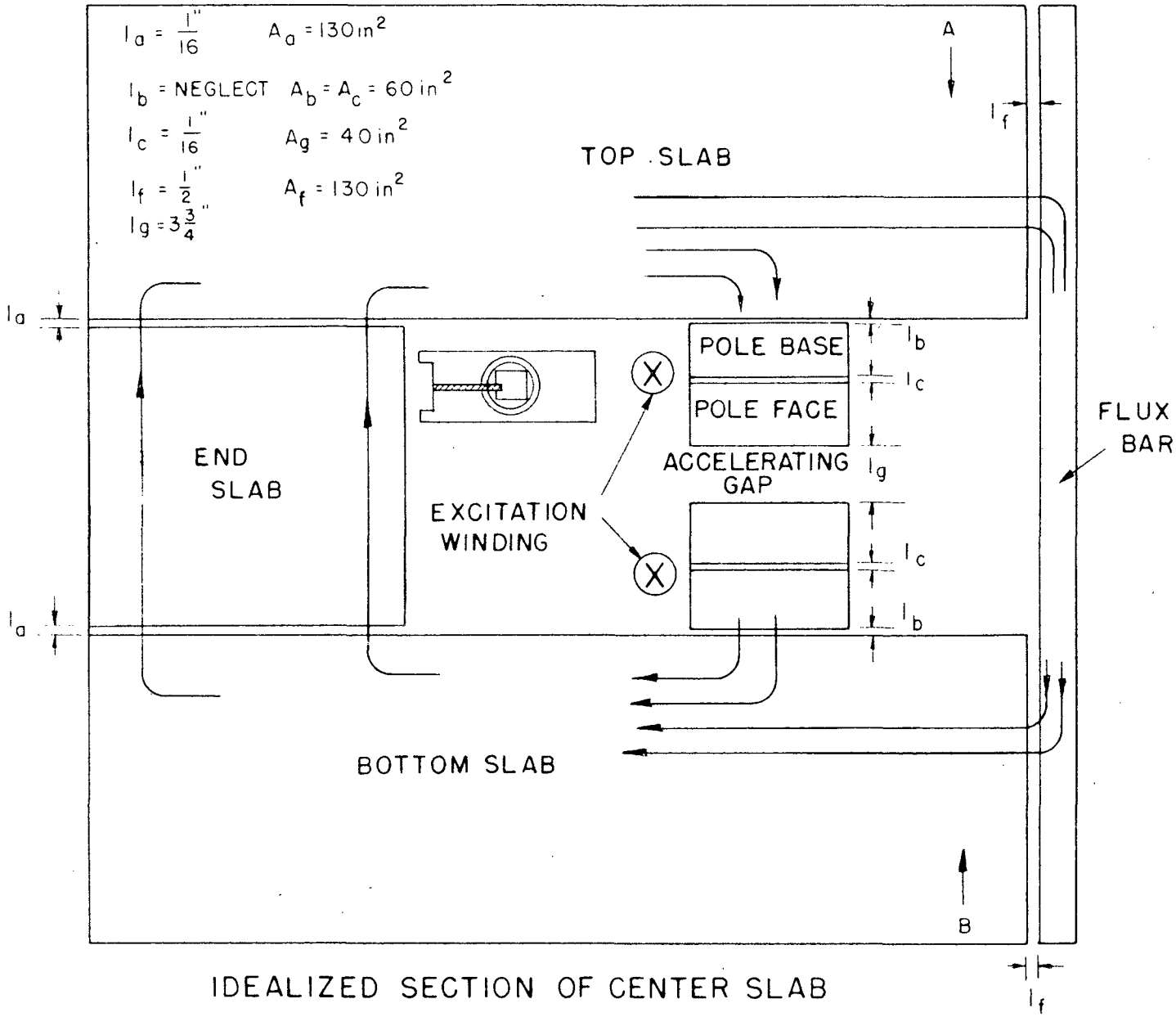

IDEALIZED SECTION OF CENTER SLAB

FIG. 15A

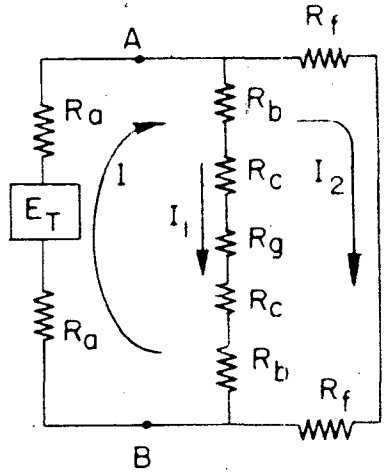

FIG. 15B

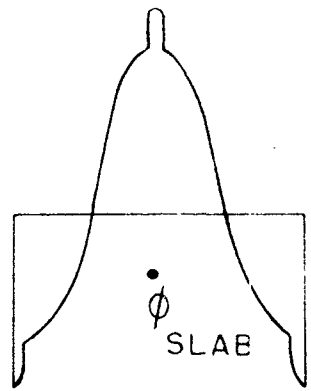

FIG. 15c

13531-1

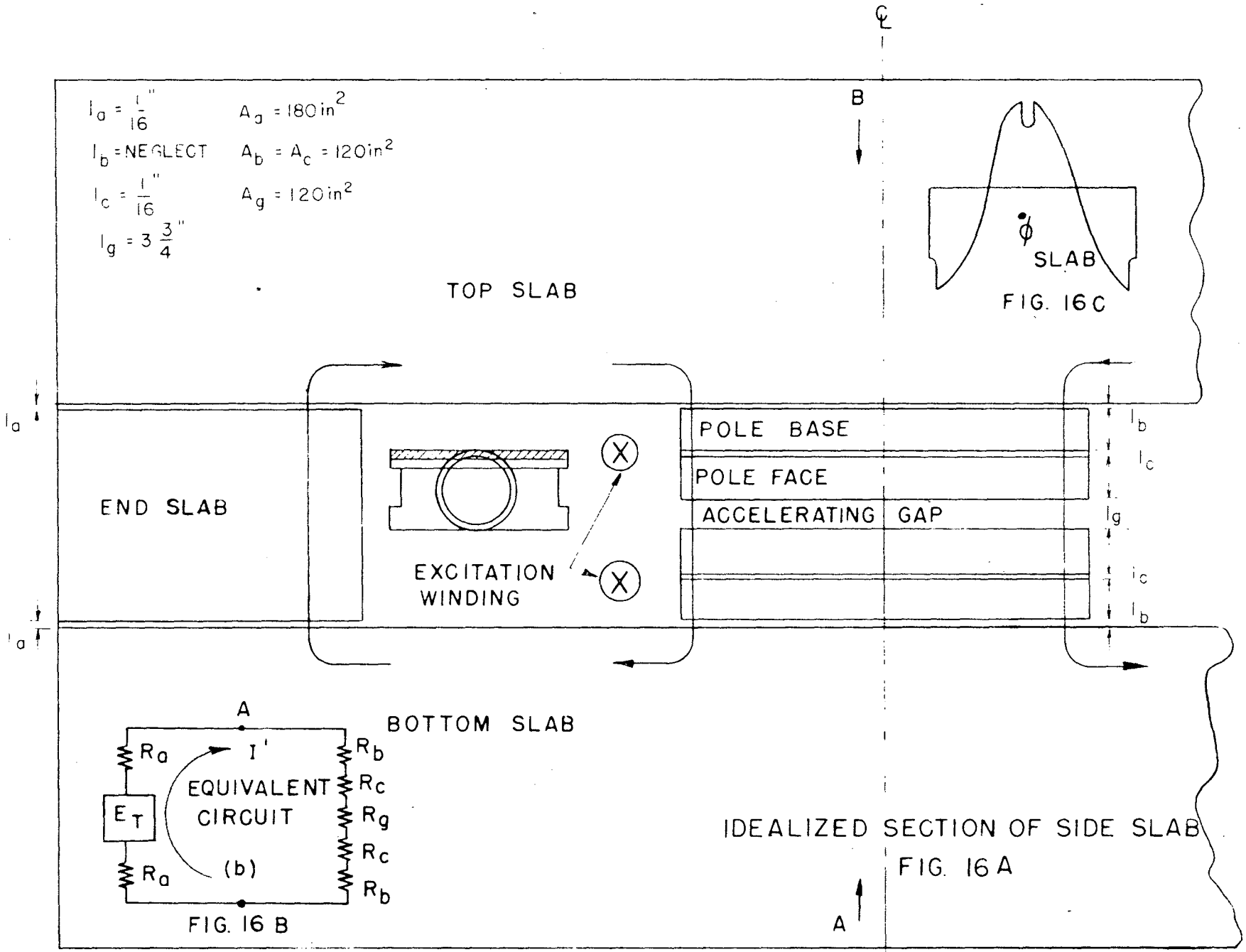
$l_a = \frac{1}{16}''$
$A_a = 180\,in^2$
l_b = NEGLECT
$A_b = A_c = 120\,in^2$
$l_c = \frac{1}{16}''$
$A_g = 120\,in^2$
$l_g = 3\frac{3}{4}''$
TOP SLAB
B
SLAB
FIG. 16C
l_a
END SLAB
EXCITATION WINDING
POLE BASE
POLE FACE
ACCELERATING GAP
l_b
l_c
l_g
l_c
l_b
l_a
BOTTOM SLAB
A
R_a
I'
R_b
R_c
R_g
R_c
R_b
R_a
E_T
EQUIVALENT CIRCUIT
(b)
FIG. 16 B
IDEALIZED SECTION OF SIDE SLAB
FIG. 16 A
A
13532-1

then: MMF is analogous to E

ϕ is analogous to I

$\mathcal{R}$ is analogous to R

Consider the first type of magnetic circuit as idealized in Fig. 15(A). From the equivalent circuit of Fig. 15(B):

$$E_T = I R_T = (I_1 + I_2) R_T$$

$$E_T = I \left[2 R_a\right] + I_1 \left[2 R_b + 2 R_c + R_g\right] \qquad (23)$$

$$E_T = I \left[2 R_a\right] + I_2 \left[2 R_f(t)\right] \qquad (24)$$

$$E_T = 2 I R_a + E_{AB}$$

where: $R_f(t)$ is variable with time. For purposes of explanation R_f will be considered to have only two values, R_{fB} during the betatron condition and infinity after the flux bar saturation.

Then: $$E_{AB} = E_T - 2(I_1 + I_2) R_a \qquad (25)$$

Now consider the second type of magnetic circuit as idealized in Fig. 16(A). From the equivalent circuit of Fig. 16(B):

$$E_T = I' R_T$$

$$= I' \left[2 R_a + 2 R_b + 2 R_c + R_g\right]$$

$$= E'_{AB} + 2 I' R_a \qquad (26)$$

$$E'_{AB} = E_T - 2 I' R_a \qquad (27)$$

As a consequence of the resistance, R_a, a portion of the potential drop appears in the return path. The proportion of E_T appearing across $2R_a$ can be computed in a rough fashion by calculating the ratio of the reluctances from their physical dimensions*. The ratio of the resistances in the equivalent circuit will have the same value. For the circuit of Fig. 15 the proportion of E_T appearing across $2R_a$ for the branch through which the current I_1 flows

*The usual definition for reluctance is $\mathcal{R} = \frac{\ell}{\mu A}$ where ℓ is the length of the gap and A is the cross sectional area. The approximate values for the various gaps are given on Figs. 15 and 16.

is:

$$\frac{E_1}{E_T} = \frac{I_1(2R_a)}{I_1(2R_a + 2R_b + R_g)} = \frac{\left(\frac{2 \times 1/16}{130}\right)}{\left(\frac{2 \times 1/16}{130} + \frac{2 \times 1/16}{60} + \frac{3\ 3/4}{40}\right)} \approx 1/3\%$$

Similarly for the branch through which the current I_2 flows:

$$\frac{E_2}{E_T} = \frac{I_2(2R_a)}{I_2(2R_a + 2R_{fg})} = \frac{\left(\frac{2 \times 1/16}{130}\right)}{\left(\frac{2 \times 1/16}{130} + \frac{2 \times 1/2}{130}\right)} \approx 11\%$$

The total proportion of E_T will be the sum of these two quantities or essentially 11 percent.

A similar analysis for the circuit of Fig. 16 yields the result:

$$\frac{E_1'}{E_T} = \frac{I'(2R_a)}{I'(2R_a + 2R_b + R_g)} = \frac{\left(\frac{2 \times 1/16}{180}\right)}{\left(\frac{2 \times 1/16}{180} + \frac{2 \times 1/16}{120} + \frac{3\ 3/4}{120}\right)} \approx 2\%$$

In this case there is only one branch to consider because there is no shunt flux bar circuit.

These rough results show a difference of about 10 percent in the potential at AB. Returning to the magnetic circuit this can be interpreted as a difference of 10 percent in the MMF_{AB} available across A-B for the two different types of circuit. This results in a 10 percent difference in the rate of change of field between the East-West and North-South axes. The measured difference in these rates of change was 11 percent as shown on Fig. 36.

BASIC METHODS OF INVESTIGATION

A. General

In order to satisfy the above requirements it was necessary that detailed and accurate investigations of the field conditions be made with a minimum of time and effort. Outlined below are the basic methods used for the various investigations and the corrections used to attain the final field.

B. Methods for Investigation

1. Search Coil Measurements

One of the basic methods of obtaining data on the characteristics of the time varying magnetic field was through the use of search coils. These are simply coils of wire with an accurately known effective area for linkage by magnetic flux. In general, if such a coil is placed in an alternating magnetic field whose amplitude is described by $B = B_{max} f(t)$, then the voltage appearing at the terminals of the coil will be:

$$E = -A \frac{dB}{dt} \times 10^{-8} = -AB_{max} \frac{df(t)}{dt} \times 10^{-8} \qquad (28)$$

A = effective area of the coil

This is the fundamental relationship from which stems the usefulness of search coils in the measurements described subsequently.

a. Maximum field measurements.

One application of such a coil was in the measurement of the maximum field. It is noted that if equation (28) is integrated with respect to time a function proportional to the total change in B is obtained. This integration can be carried out electrically as discussed in appendix B and the resultant voltage displayed on a CRO*. The waveforms obtained for our magnetic field are shown in Fig. 12.

b. Comparison of two fields.

A second application of search coils was in the comparison of

*The abbreviation CRO will be used throughout for Cathode Ray Oscilloscope.

two fields. If two identical search coils are placed in identical time varying fields and their outputs placed in series opposing and integrated* the resultant signal will be zero. More generally if the coils have areas $A_2 > A_1$ and A_2 is placed on a goniometer in some fixed reference field and A_1 is free to move in the field to be analyzed, then an accurate method of measuring small differences in field magnitudes is provided#. If the coils are placed, one over the other, and the goniometer coil rotated from its maximum effective area position until the resultant signal is zero, then

$$A_1 B_1 = A_2 \cos\theta\, B_2$$

but $$B_1 = B_2$$

hence $$A_1 = A_2 \cos\theta_R$$

and for any other point of the field

$$\frac{B_1}{B_2} = \frac{\cos\theta}{\cos\theta_R}$$

Since A_1 and A_2 and θ_R are known the ratio B_2/B_1 can be obtained for all points in the desired region and hence if one absolute value of B is obtained for any one of these points, all points can be directly deduced. Appendix C elaborates this method.

c. Betatron condition measurements.

A third application of search coils was in the investigation of the betatron acceleration condition. As previously stated the condition which must be satisfied is $\dot{\Phi}_o = 2\pi r_o^2 \dot{B}_o$. This is most easily accomplished by comparing two voltages, one of which is proportional to $\dot{B}_o$ and the other proportional to $\dot{\Phi}_o$. Such voltages are obtainable by using a search coil on the orbit and a single turn of wire coincident with the orbit. The former

*Mathematically this is the same as integrating each voltage separately and bucking the resultant outputs because, for continuous functions, $\int (a+b)dt = \int a\,dt + \int b\,dt$. The method mentioned above eliminates the difficulty of constructing identical integrators.

#See Appendix B.

has a voltage proportional to the rate of change of field in the gap and the latter a voltage proportional to the rate of change of the flux enclosed. Appendix D elaborates these relations and indicates that during the betatron period the two voltages are related by a constant:

$$\frac{E_{sc}}{E_{oo}} = K = \frac{A_{sc}}{2\pi r_o^2} \qquad (29)$$

Then if the single turn orbit coil voltage is attenuated (it being the larger of the two voltages) by this constant and placed in series opposing with the search coil voltage a resultant voltage of zero should be obtained when the conditions are satisfied.

2. Peaking strip measurements

A second basic method for obtaining data was by means of peaking strips. Because of the very low field strength required to saturate a strip of permalloy (approximately .1 oersted), a coil of wire wound around such a strip will have a voltage pulse induced in it as the field variation goes through the zero field point.* If two such peaking strips are placed in the magnet at points where the magnetic fields do not pass through zero field at the same instant, the phase difference between these two points may be measured directly be applying both to the vertical deflection plates of a synchroscope with a suitable sweep speed. This method may be extended to field strengths other than B = 0 by biasing the peaking strip coils with a direct current from an external source. This superimposes a d-c magnetic field on the time varying field due to the magnet. The output pulse will then occur when the instantaneous algebraic sum of the two fields is zero. This procedure allows a direct measurement, in time, of phase differences around the orbit and this may be converted to magnetic field when the rate of change of field of the magnet is known.

*See Appendix E.

PRELIMINARY INVESTIGATIONS AND OBSERVATIONS

The design of the magnet and associated components affecting the magnetic field will not be dealt with in detail. However, a summary of the important investigations is presented below.

A. D. C. Model Tests

The design of the magnet yoke and pole pieces was determined on d-c models. Initial measurements were made on a crude preliminary model as shown in Fig. 17, which was soon replaced by an accurate 1/8-scale model. This was Model A shown in Fig. 18. Several different pole face geometries were investigated in this model and on the basis of the data obtained Model B, also 1/8-scale, was built. The geometry of Model B was that used in the final magnet. It is shown in Fig. 19. Several further pole face variations were required before the desired combination was achieved. The object of this painstaking and rather tedious development was to get the maximum volume of useful field with a minimum volume of iron. This was desirable as it reduced the amount of iron, the required magnetising current and the kva rating of the capacitors simultaneously.

The final full scale pole face geometry selected is shown in Fig. 6 and the field variation with radius is plotted in Fig. 20. The model data was checked with a full scale assembly and found to be valid.

B. A. C. Models and Tests

1. Preliminary Model

The first a-c model was built for continuous operation with sixty cycle excitation and had two hypersil iron cores as shown in Fig. 21. This magnet was used for some preliminary qualitative observations.

2. Model ACR-1 1/2

The above model was replaced by Model ACR-1 1/2 which had four laminated hypersil cores as shown in Fig. 22. The laminations were bonded

PRELIMINARY MODEL (D. C.)
FIG. 17

MODEL A
(D.C.)
FIG. 18

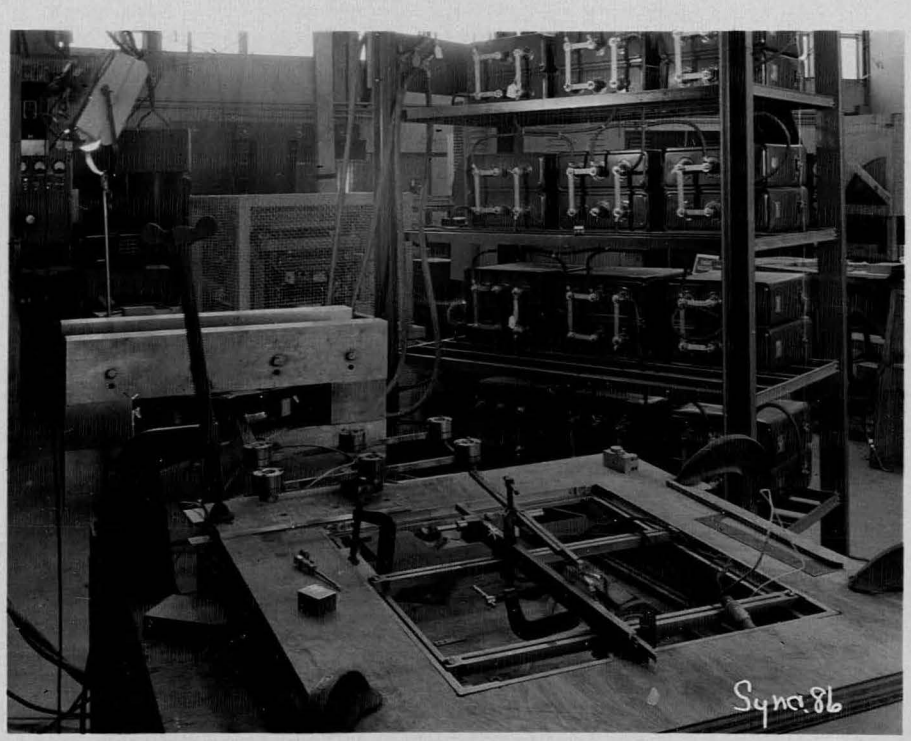

MODEL B (D.C.)
(IN BACK OF LARGE CLAMP)

FIG. 19

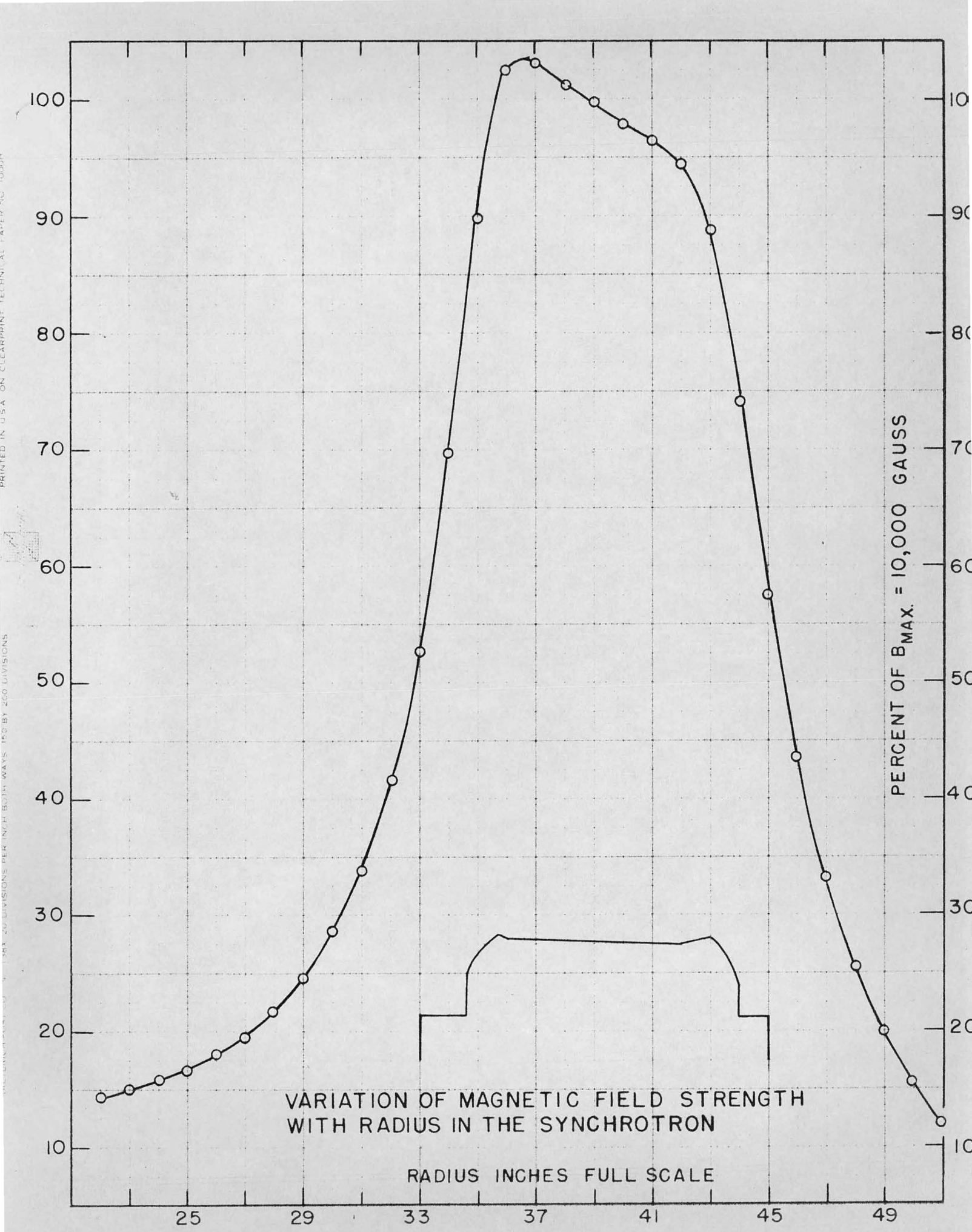
100
90
80
70
60
50
40
30
20
10
PERCENT OF $B_{MAX.}$ = 10,000 GAUSS
VARIATION OF MAGNETIC FIELD STRENGTH
WITH RADIUS IN THE SYNCHROTRON
RADIUS INCHES FULL SCALE
25
29
33
37
41
45
49

FIG. 20

B533-1

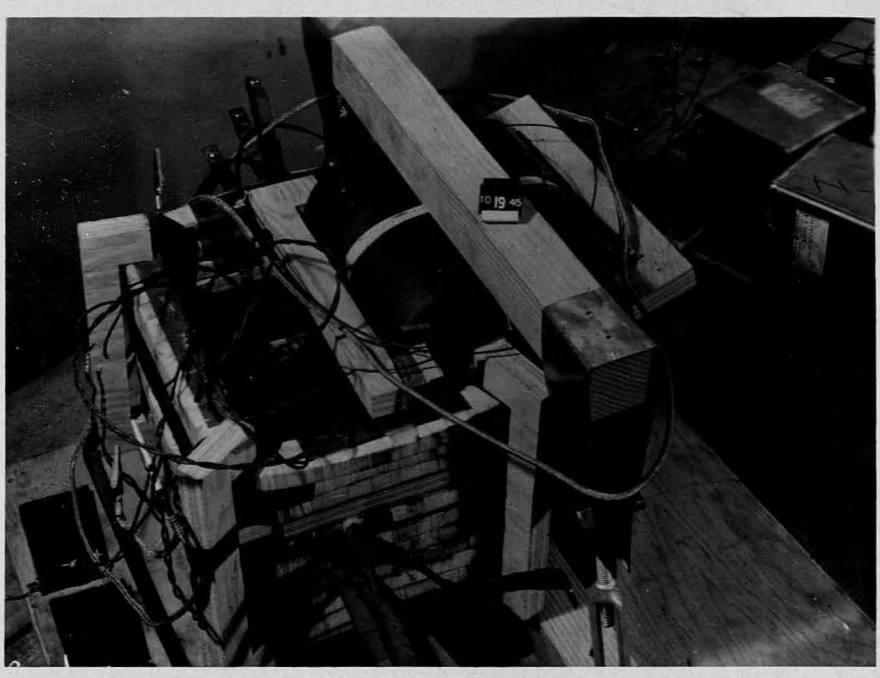

PRELIMINARY A.C. MODEL

FIG. 21

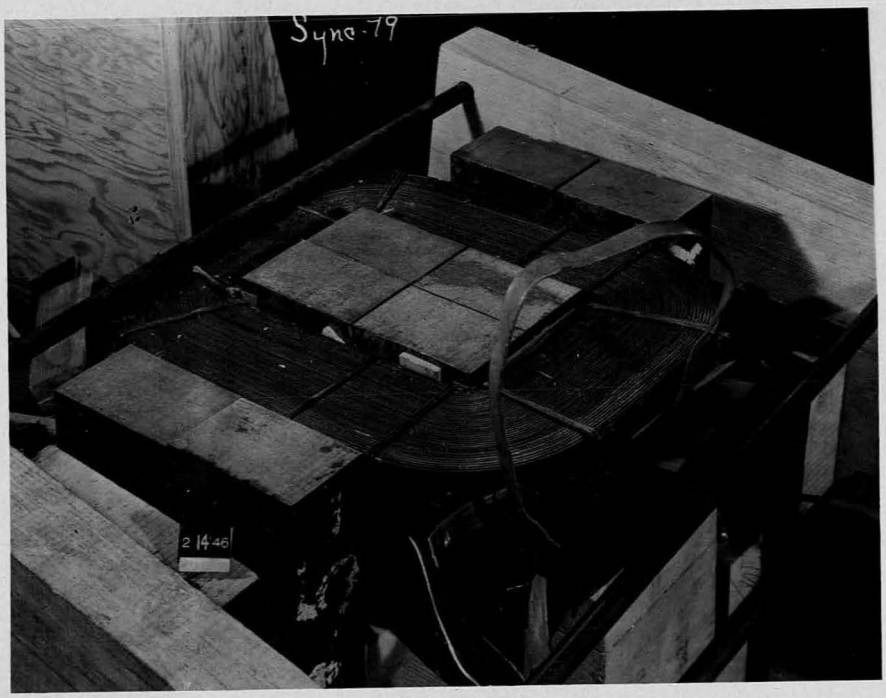

MODEL ACR – $1\frac{1}{2}$

FIG. 22

with redux cement, which was chosen from samples of several different bonding materials on the basis of comparative tests. It is interesting to note that only two of the various samples tested failed to break down mechanically when the magnet was pulsed. This model could be operated continuously or pulsed by a circuit similar to the one used in the final synchrotron. A number of investigations were made on this model including the effect of eddy currents in the dee structure* on the magnetic field at the orbit and the effect of the copper foil lining of the plastic rings. Also studied was the effectiveness of equalizing coils in obtaining phase lags.# This was done by winding a coil around one of the four hypersil cores of the magnet and connecting a resistance across the coil terminals to control the induced current. The results indicated that phase lags of rather large values may be obtained without difficulty and that the area of influence of the coil was markedly larger than the segment around which it is wound. The latter effect was not nearly so pronounced in the full scale magnet.

3. Model AC-1/2

This was a 1/8 scale model of a 1/8 section of the full scale machine and was fabricated from the same iron and with the same techniques. Its excitation source was also similar to that of the full scale machine which allowed observations of its behavior under pulsed operation. The model and power supply are shown in Figs. 23 and 24. On this model the design of the flux bars was completed and the betatron condition studied in some detail to postulate methods for improving the critical early stages

*The original design of the synchrotron called for a copper dee structure for applying the r.f. voltage which was inside the plastic rings used as the walls of the vacuum chamber. The effect of eddy currents in these dees was an important problem in this system.

#See Appendix F.

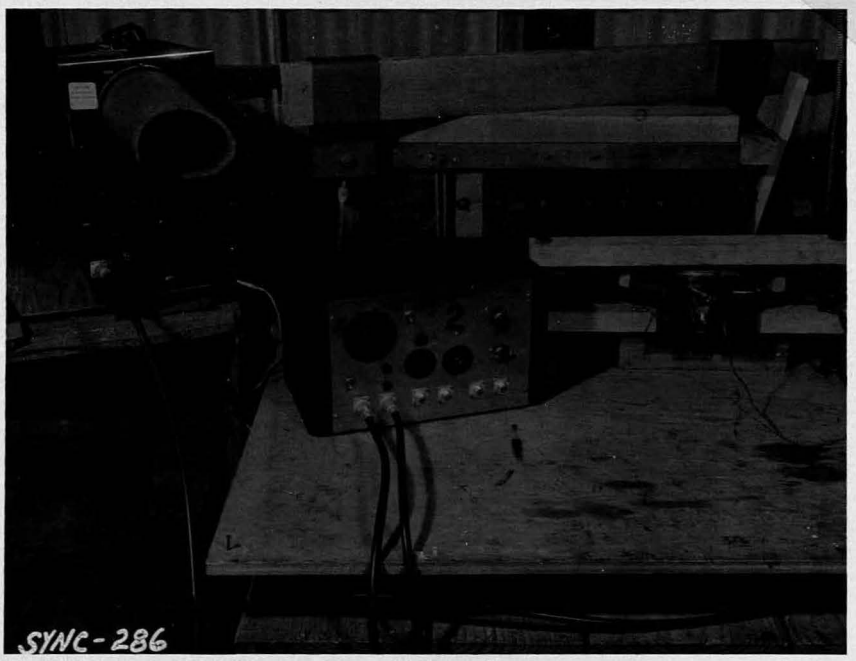

MODEL AC – $\frac{1}{2}$

1 MODEL
2. AMPLIFIER INTEGRATOR

FIG. 23

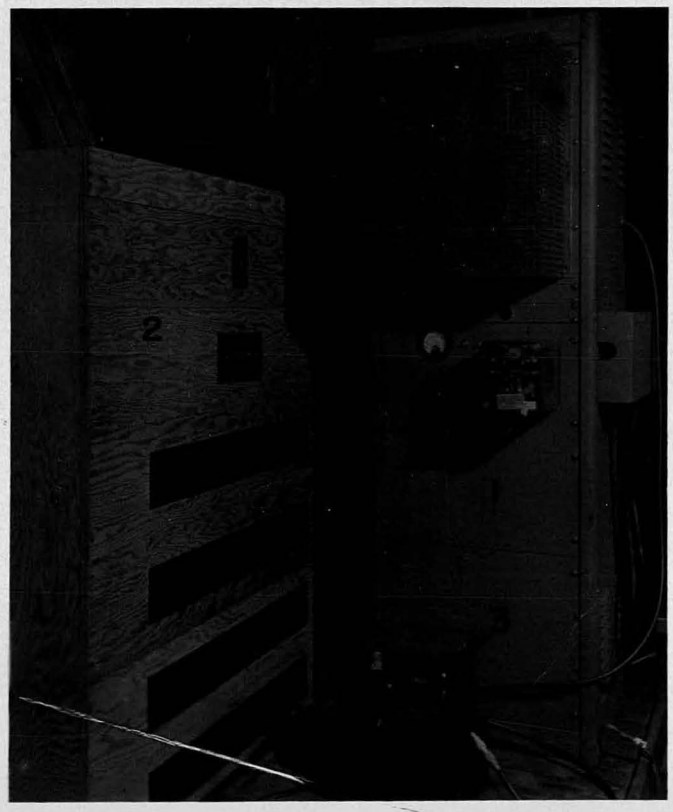

MODEL MAGNET PULSER

1. POWER SUPPLY AND THYRATRONS
2. CAPACITOR BANK
3. TRIGGER GENERATOR

FIG. 24

of acceleration between the injection and the r.f. turn on times. A summary of the predicted and verified results of this study is given below.

a. Flux bar study.

A study of the flux bars, particularly their action in increasing the flux through the orbit; decreasing the rate of change of field on the orbit and change in the effective inductance of the magnet.

b. D-C Flux bar bias.

A d-c bias field induced in the flux bars moves the betatron condition with respect to the magnetic cycle. This can be accomplished by a single turn loop around the flux bars in which a direct current is circulated. The bias field will be proportional to the current flowing.

c. Search coil design.*

Considerable time was spent in designing a search coil of small physical size capable of producing a large enough voltage to be efficiently integrated. The particular coils designed at this time were quite satisfactory in the model but due to different transient conditions in the full scale machine had to be modified with slightly less rigorous demands.

d. Peaking strip design.

Peaking strips of various forms have been used for other applications and in other similar machines, though not in so refined a form.[10] Their function in the actual operation of the synchrotron is to trigger the electron injector and the r-f oscillator at the proper absolute value of magnetic field independent of any time scale. A second important application, already mentioned, is in the determination of small phase differences in the azimuthal field. The preliminary observations on, and the design of, the test peaking strips was done with the model magnet and

---

*It was at this time that the author joined the project.

[10]See bibliography.

with the experience gained, a suitable design was found for the operating trigger strips which were much longer than the model magnet gap. The test peaking strips could be only 3/8 inches long in order to fit in the model magnet gap. The requirements of the output signal was that it have a very fast rate of rise and as large a voltage output as possible. Among the problems encountered in designing a practical strip was the one of winding the wire on the permalloy core. The voltage output is:

$$E_p = -N \frac{d\phi_p}{dt} \times 10^{-8} \qquad (30)$$

N = number of turns in the coil.

ϕ_p = flux in the permalloy.

There is also a second voltage induced in the coil:

$$E_B = -A \frac{dB}{dt} \times 10^{-8} \qquad (31)$$

A = effective area of the coil for magnetic flux.

B = magnetic induction field outside of the permalloy but threading the coil.

This latter voltage is undesirable and unless $E_B \ll E_p$ the identity of the peaking strip pulse may not be well defined and the rise time will be too great. The area, A, was minimized by using very small wire (42 B & S gauge) for the winding and further by the use of a machine whereby the winding was placed directly on the permalloy core with a minimum possible are enclosed. By these techniques it was possible to wind 500 turns of wire with a negligible effective area.

The peaking strips showed the following general characteristics:

(1) The pulse amplitude increases with increasing N.

(2) The pulse amplitude increases with increasing cross-section of permalloy.

(3) The pulse width decreases with increasing length of permalloy core.

(4) The pulse width increases with increasing cross-section area.

(5) The pulse width decreases if the coil is placed in a region near the center of the permalloy and is short compared to the length of the permalloy.

It would appear that (2) and (4) are in opposition, however, the effect of (4) is due to eddy currents which can be materially reduced by the use of laminated cores. (3) and (5) are somewhat similar effects having to do with the fact that the leakage flux near the center is reduced by increasing the length of the permalloy and the rate of change of flux is a maximum where the leakage is a minimum.

The final design is shown in Fig. 25 and its output signal as viewed on a synchroscope is shown in Fig. 26. The core consists of two laminations of .001 x .010 inch permalloy insulated by a glyptal film. The rate of rise of the steepest portion of the leading edge is about .5 volts per micro-second. No jitter is detectable on a one micro-second per inch sweep on the synchroscope. The coil has 500 turns of 42 B & S gauge wire.

In the full scale machine the design was varied by making the permalloy core one inch long (for the reasons put forth in (5) above) and separating the laminations with cellulose tape. Difficulty is encountered in using narrow widths of permalloy because they are not available commercially and shearing after heat treatment inevitably leads to a decrease in the effective permeability. Rough calculations indicate that for a .010 inch width the effective permeability is approximately 1000 which is about 2 percent of that for the commercial permalloy from which the strips were cut. This includes the effect of stray capacity and the loading of the peaking strip coil which are not easily distinguishable.

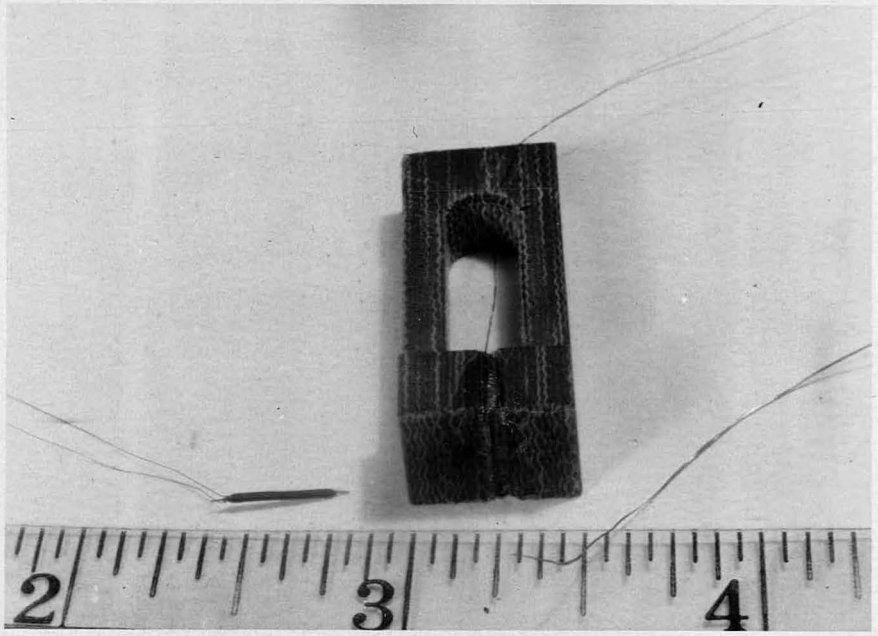

PEAKING STRIP AND MOUNT

FIG. 25

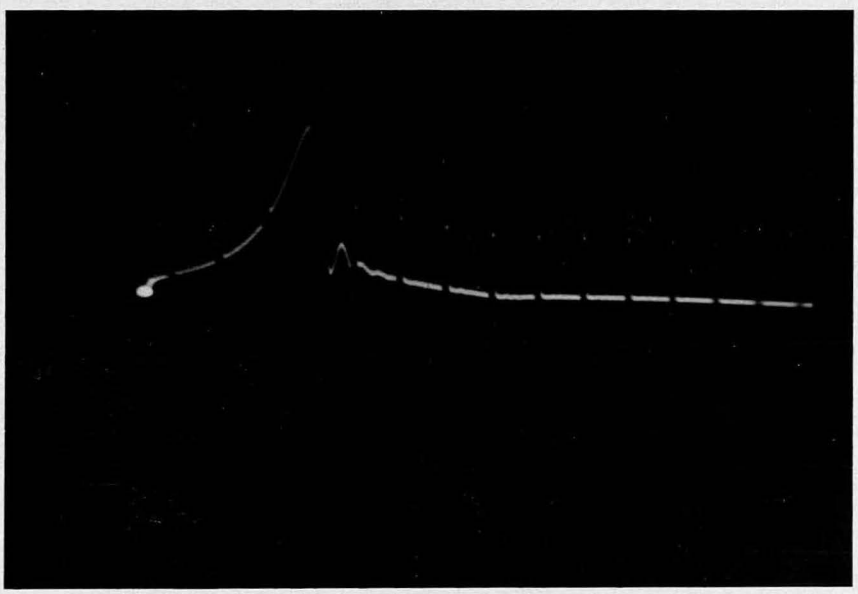

PEAKING STRIP OUTPUT VOLTAGE WAVEFORM
2 MICRO-SECOND MARKERS, AMPLITUDE = 3.6 VOLTS

FIG. 26

Experiments to determine the effect of rotating the peaking strip in the field show that its vertical positioning is critical only to about 10 degrees of arc. For angles of inclination of the axis of the core with respect to the field lines greater than 10 degrees a shift in time phase is noted due to eddy currents in the permalloy.

EQUIPMENT

A. General

As a result of calculations, experiments and general design procedure, considerable equipment was assembled to augment and facilitate the investigations and adjustments described above. This equipment was in many respects similar for the separate tests and it was desirable to coordinate the various tests so that they could be made as nearly simultaneous as possible. The equipment was roughly divided between two locations. The first was in the field proper or near it and consisted of the probing and pickup devices and associated equipment. The second location contained the analyzing and controlling equipment and was located about twenty feet from the magnet.

B. Field Equipment

The pickup equipment in the field has been described previously. To obtain the single turn orbit loop and adequate means for positioning the search coils and peaking strip coils as required, a temporary track structure made entirely of textolite was built. One of the problems of precise magnetic measurements is to obtain data without affecting the field locally with the pickup devices. This is particularly true of time varying magnetic field measurements because in any conducting material introduced in the field eddy currents will be induced, which in turn cause phase lags locally. Such local variations, even though small, could seriously affect the accuracy of measurements because we were interested in variations of a few tenths of a gauss. For this reason the entire supporting and positioning system was fabricated from non-magnetic non-conducting materials, principally textolite. The track structure, shown in Fig. 27, was assembled inside the vacuum chamber before the top section of the magnet yoke was installed and removed after the tests were completed before the quartz donut was installed.

The track assembly consisted of a fixed track which supported and positioned accurately a mobile ring. The ring could be rotated by means of a belt in a V-groove. The track and the ring were each composed of sixteen identical sections connected together in a circle by junction plates. The fixed track was positioned by secondary supports which were in turn clamped by a primary support which bolted directly to the ports of the vacuum chamber. The separate components of the system are shown in Fig. 28. Accurate positioning of the track was obtained by radial and vertical adjustment of the secondary supports. For ease of operation of the mobile ring on the track, two "ways" were milled onto the horizontal surface and forty-eight wheels installed to bear on the inner vertical surface of the ring as shown in Fig. 27. The extreme radius was marked in 1/4 inch intervals for locating any azimuthal position accurately. A V-groove was milled in the central vertical surface for the single turn orbit loop. The search coils and peaking strips were mounted on the track with plastic screws. The leads of each of these coils was a twisted pair of fine wire sheathed in transflex tubing and clamped securely to the ring. These twisted pairs passed out through a designated port and were connected to coaxial cable plugs for final distribution. Besides this mobile equipment there were four permanent peaking strips for use as triggers and a reference coil goniometer mount shown in Fig. 30. The system is shown diagrammatically in Fig. 29.

C. Interconnections

The interconnections between the synchrotron position and the remote operating position consisted of a series of coaxial cables, the systems being otherwise independent.

D. Analyzing Equipment

The equipment at the analyzing position was for the most part

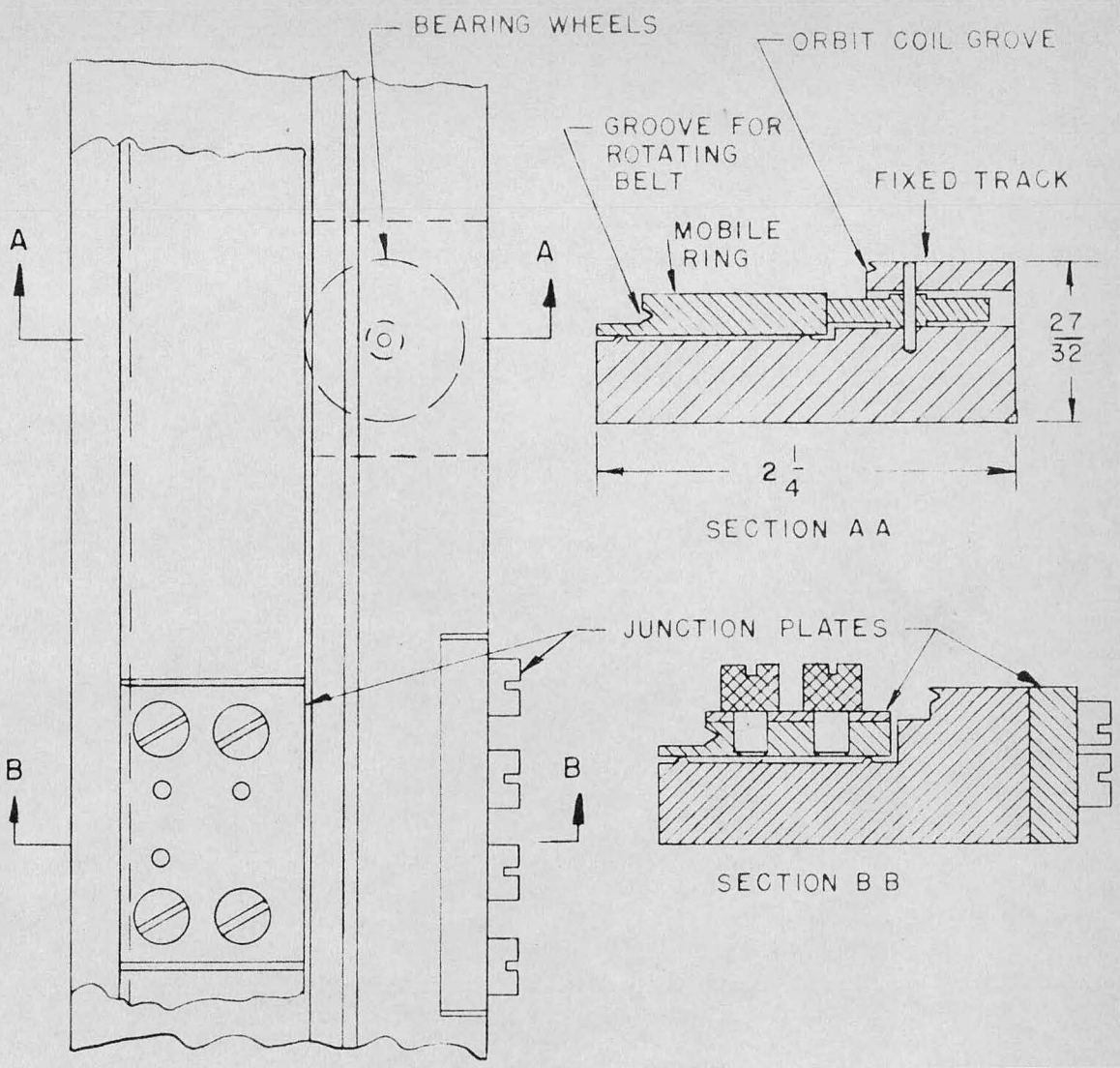

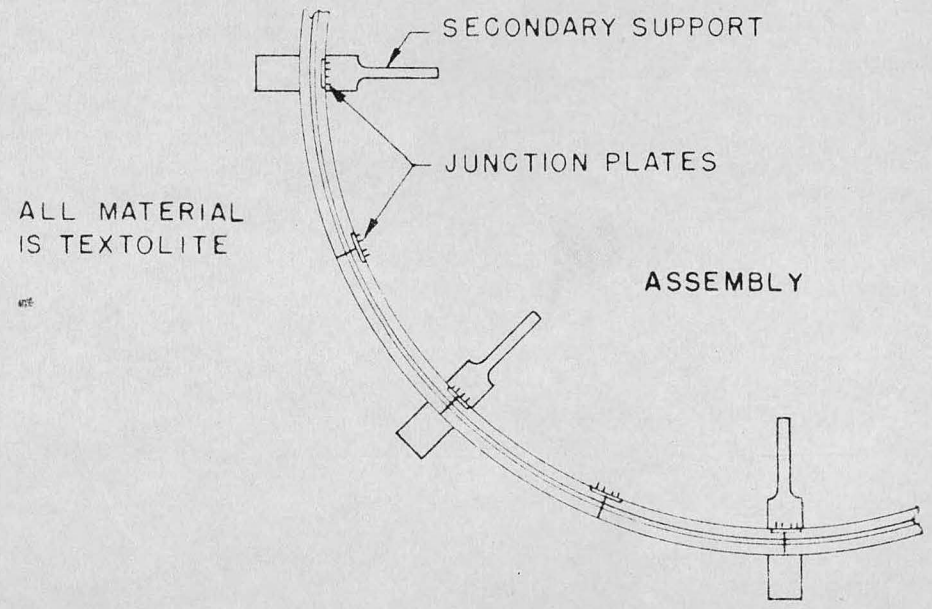

FIELD MEASURING TRACK

FIG. 27

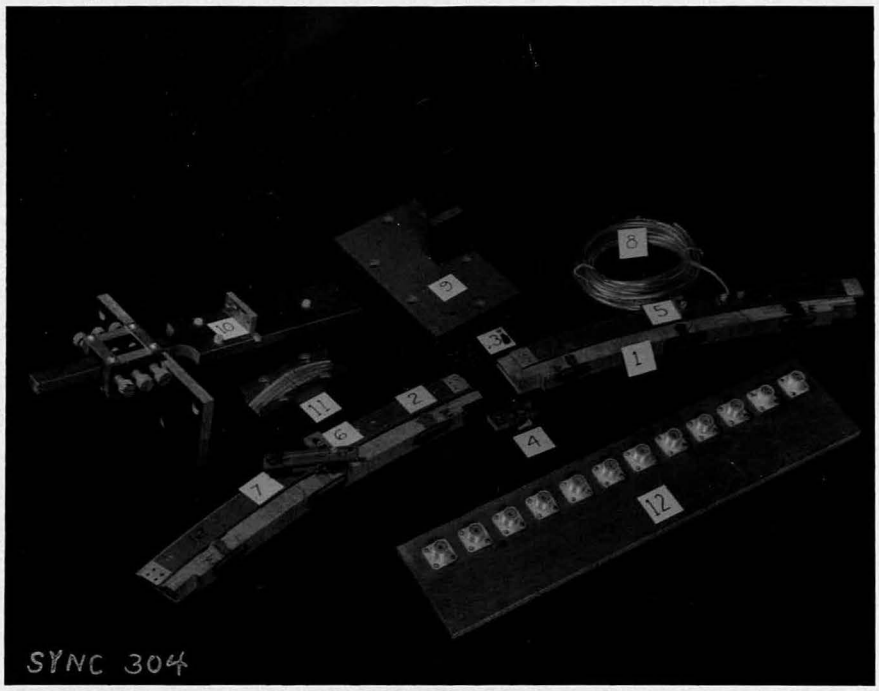

1. FIXED TRACK
2. MOBILE RING
3. RING JUNCTION PLATE
4. TRACK JUNCTION PLATE AND PLASTIC SCREW
5. PEAKING STRIP HOLDER
6. SEARCH COIL HOLDER (OBSOLETE)
7. SEARCH COIL (OBSOLETE)
8. TWISTED PAIR CONDUCTORS
9. TRACK SUPPORT IN R.F. DEE (OBSOLETE)
10. TRACK SUPPORT (USED AT ALL SUPPORT POINTS)
11. FIXED PEAKING STRIP MOUNT
12. JUNCTION PANEL FOR COAXIAL CABLES AND TWISTED PAIRS

FIG 28

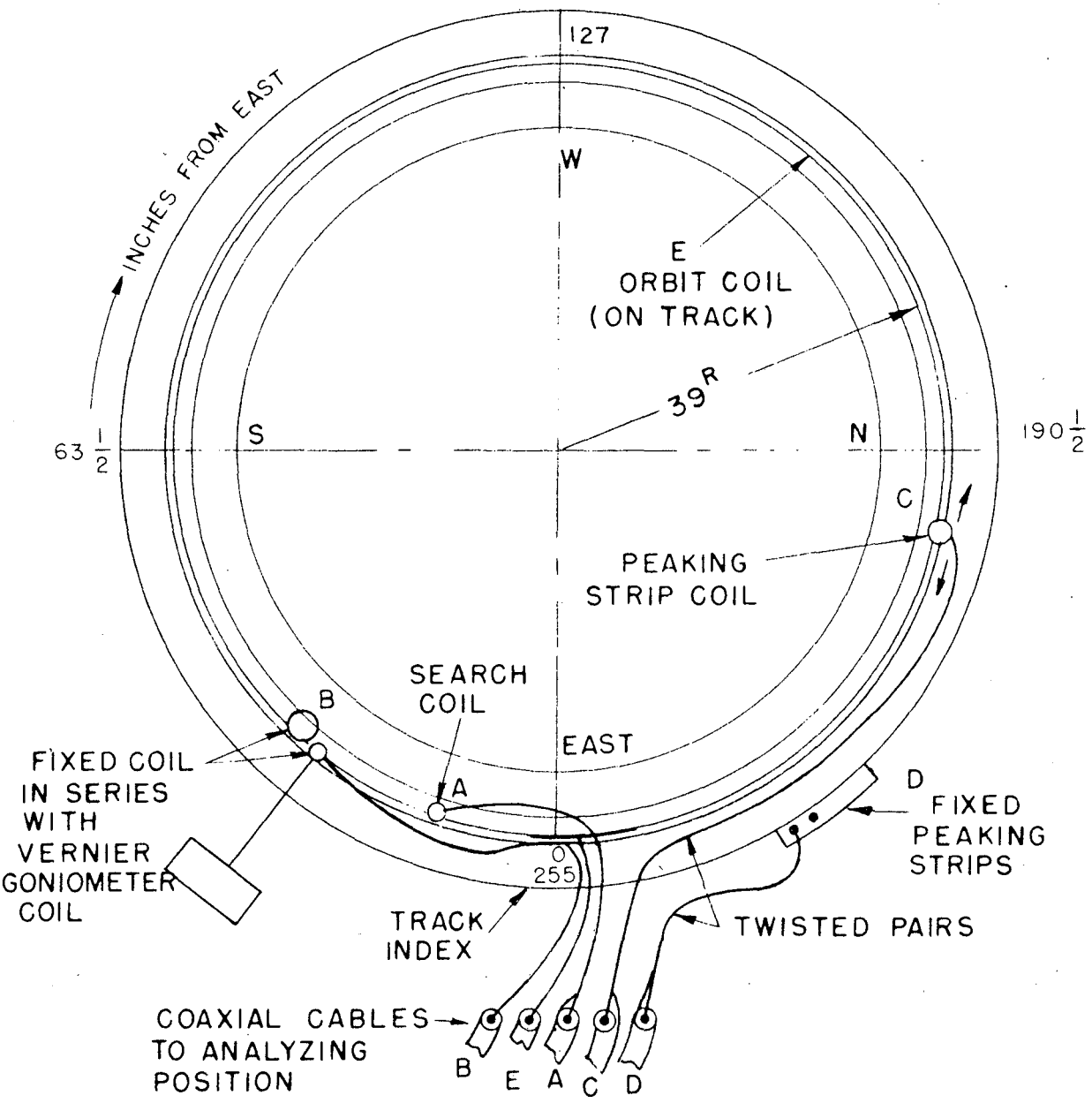

FIELD MEASURING EQUIPMENT

FIG. 29

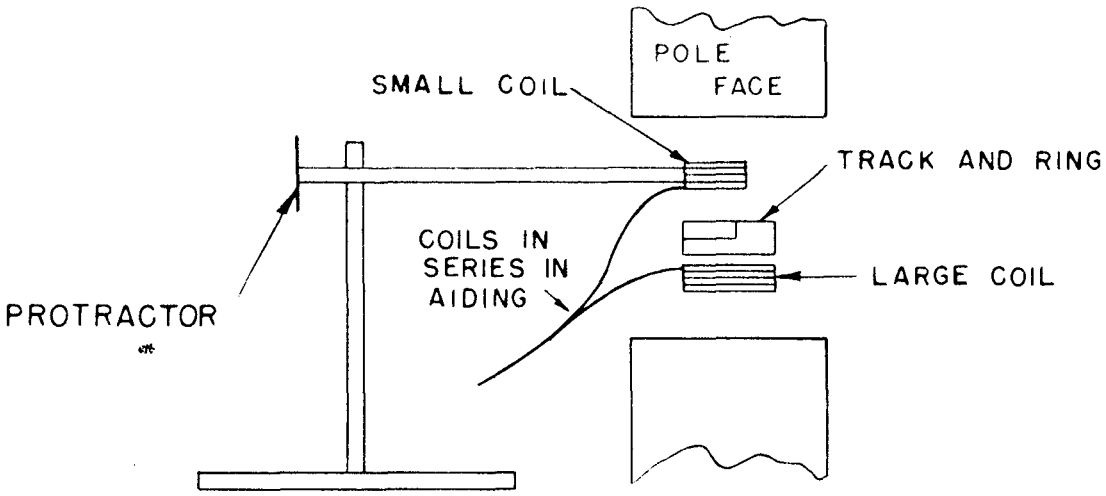

GONIOMETER

FIG. 30

standard cathode ray oscilloscopes and synchroscopes. The following list details the types of CRO and auxiliary analyzing equipment used.

Du Mont Type 208 oscilloscope modified for use with an external trigger.

Du Mont Type 248 synchroscope.

TS-28/UPN radar synchroscope.

Furzehill Type 1684D oscilloscope with d-c amplifiers.

Amplifier-Integrator Unit (see Fig. 31).

Orbit coil attenuator (see Fig. 35A).

Peaking strip bias supply.

The use of these various instruments will be detailed in a later section.

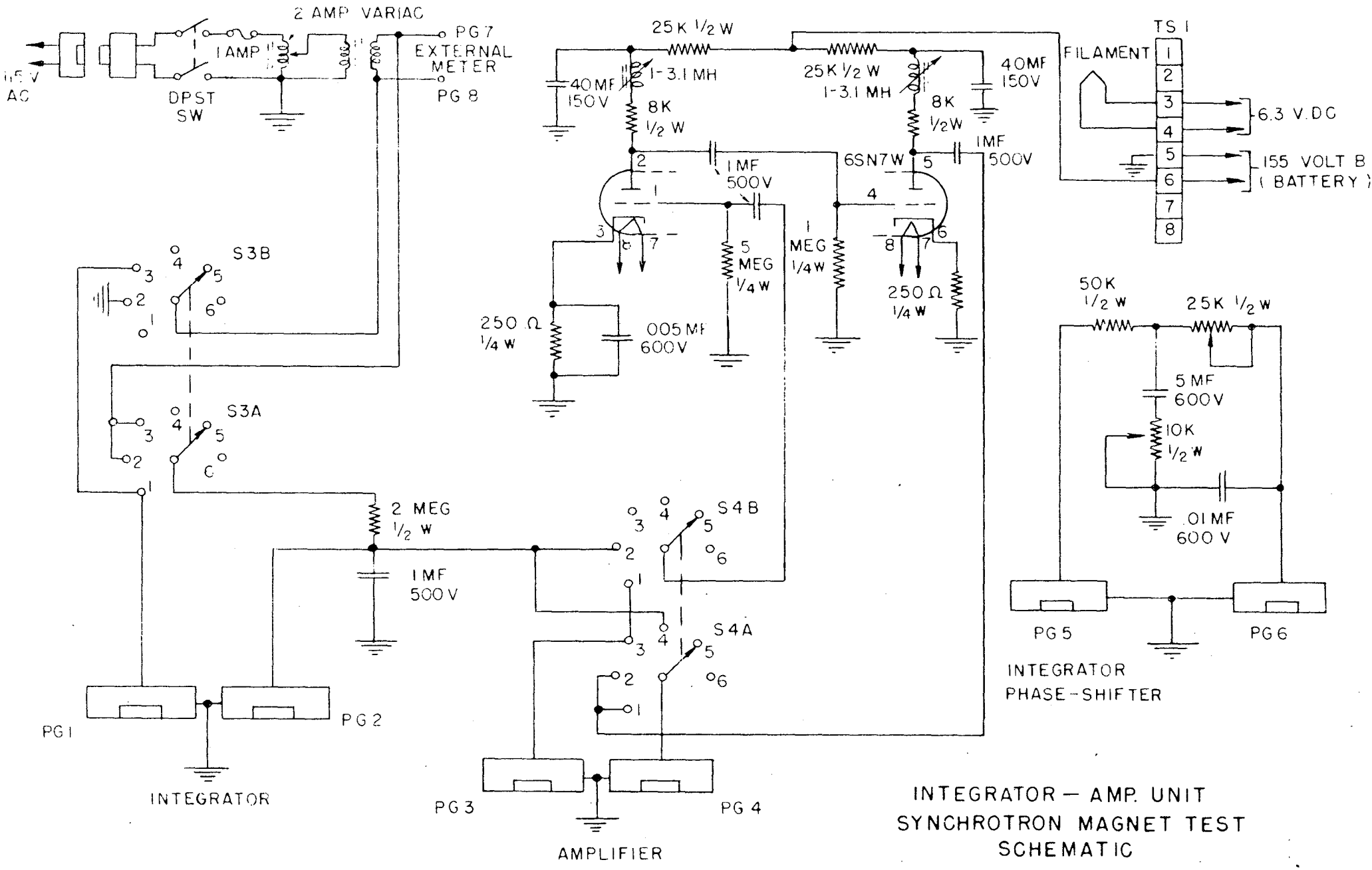

INTEGRATOR — AMP. UNIT
SYNCHROTRON MAGNET TEST
SCHEMATIC

FIG. 31

13607-1

ADJUSTMENT PROCEDURE

A. General

The basic methods to be applied to the field measurements have already been set forth in an earlier section and it remains to make an explicit account of the application of these methods to the adjustment of the magnetic field in the Berkeley Synchrotron.

The magnet is so designed that the top portion of the yoke is a single unit which is set in place as the last step of the assembly. It was predicted, and experience has corroborated, that the removal and replacement of the top yoke could be accomplished to an accuracy which would not materially affect the magnetic field conditons. This allowed the installation of the field measuring track and associated equipment in the magnet gap without the quartz donut in position. After the measurements were completed the top yoke was lifted off, the field measuring equipment removed, and the quartz donut installed.

In measuring time varying magnetic fields considerable care must be taken in the physical geometry of the electrical circuits so as to minimize voltages induced by the magnetic field which might alter the results obtained. Particular care must be taken to see that no loops which may be threaded by flux are allowed. For this reason twisted pair conductors were used exclusively in and near the magnet gap and coaxial cables in all other circuits. Also only one ground point was used in any particular circuit to avoid possible flux linking loops. Some elementary tests were run on the model magnet to check the effectiveness of the system designed and no difficulty was anticipated or encountered.

B. Maximum Field Measurements

No direct adjustment was provided for the azimuthal variation of the maximum induction field but an investigation was made and the results

are plotted in Fig. 32. Two systems of bucking coils were placed on the orbit, one for the goniometer at a fixed azimuthal position and the other on the mobile ring. The goniometer system was made up of two coils, one having an area about 8 percent less than the search coil on the ring and the other about 14 percent of this area. The large one was mounted under the track on the same vertical axis as the small one. The small one was mounted on the goniometer shaft. This allowed a vernier adjustment of a little more than $\pm$ 5 percent of the field at the goniometer position. As indicated in Fig. 32 the maximum deviation of the field is about 1.3 percent from the average. This was not considered to be outside the allowable tolerances. All of the coils used were made of a single layer of 29 B & S gauge Formvar covered magnet wire wound on carefully machined canvas bakelite forms. The areas were calculated from the physical geometry. The output voltages of these two systems of coils were connected in series bucking, integrated and presented on the Du Mont Type 208 CRO triggered in synchronism with the magnet. The circuit is shown in Fig. 33. Using the preamplifier in the Amplifier-Integrator unit(Fig. 31) to obtain very high amplification, the goniometer was rotated until the trace was most nearly a straight horizontal line near zero field. A complete cancellation of voltages for the entire cycle cannot be achieved practically because of the variation in the phase and the rate of change of field with azimuth. A zero point for the goniometer was established by presenting only the voltage of the small coil on the CRO and rotating it until a voltage minimum was obtained. The reference zero point was exactly 90 degrees from this position. The angle through which the goniometer was rotated from its zero position in order that the two coils enclose the same number of flux lines was read accurately from the vernier protractor. This data was obtained for each ten inch increment of azimuth around the orbit. The effective area of the goniometer coil was calculated from the angle

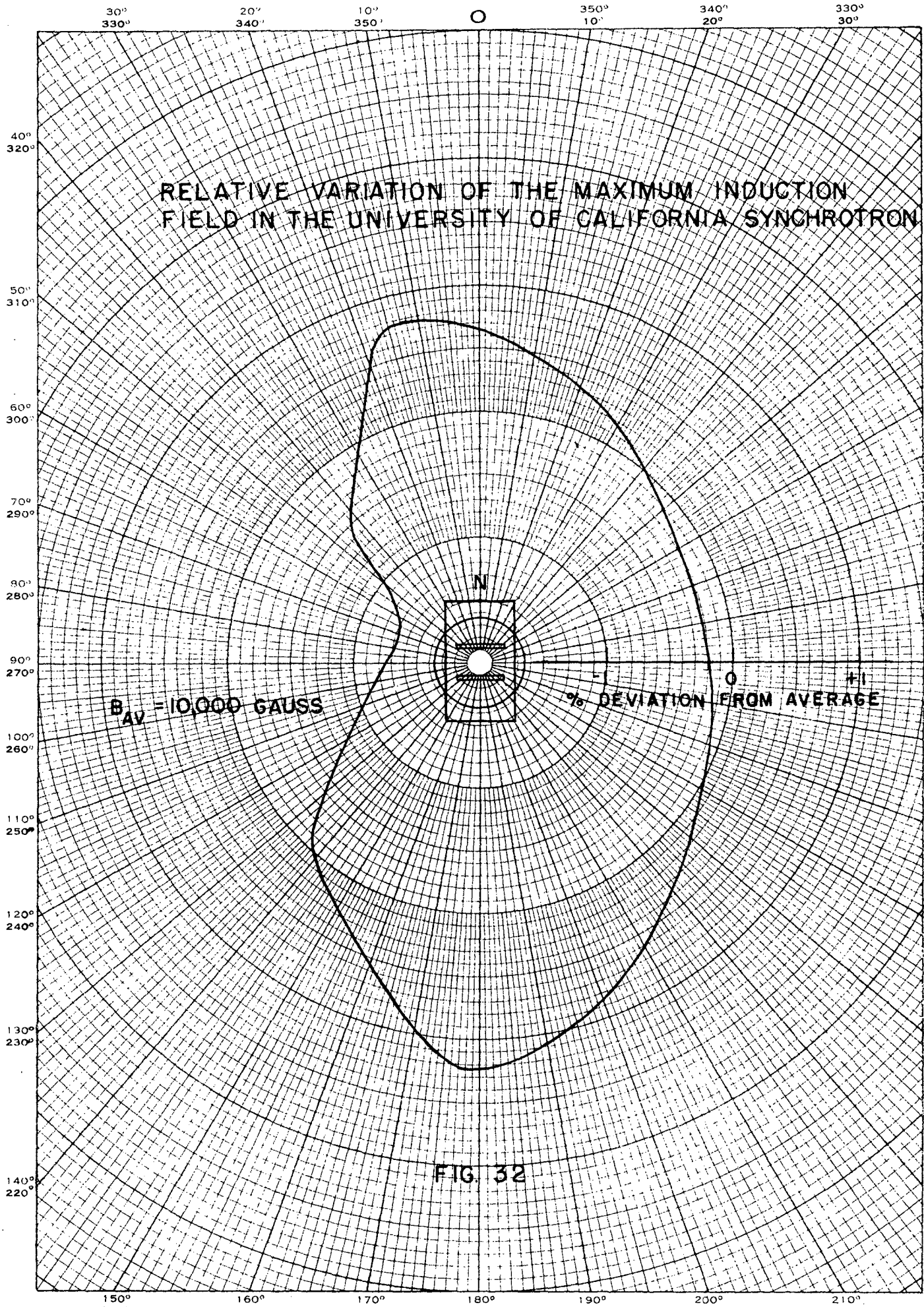

FIG. 32

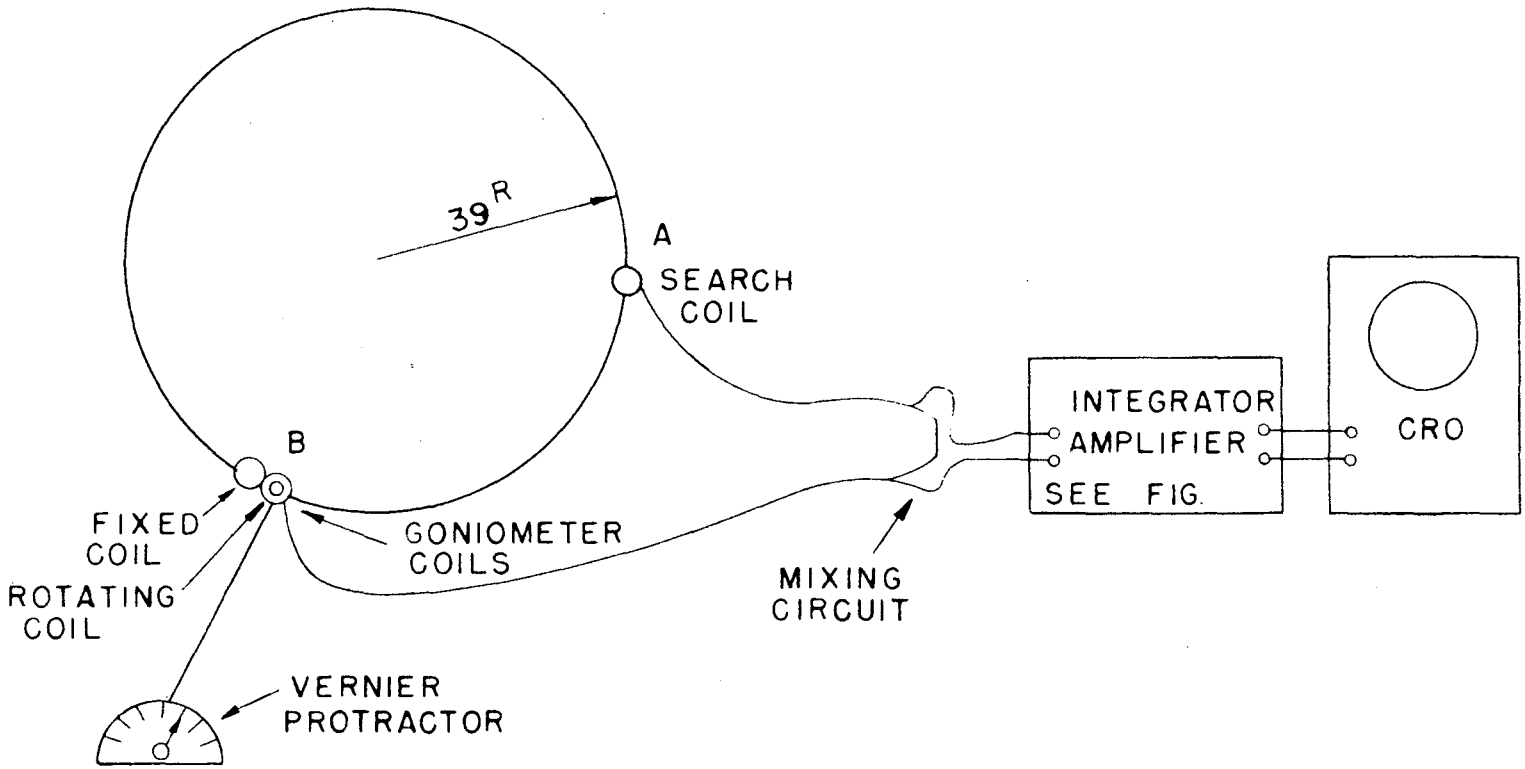

FIELD MAGNITUDE MEASURING CIRCUIT

FIG. 33

through which the small coil was rotated. By normalizing separate reading to the point where the search coil and goniometer coils had coincident vertical axes a plot of relative maximum induction was obtained. In order to calibrate this curve on an absolute scale, a single coil was used at the goniometer position, its output integrated and calibrated as set forth in Appendix B. From this value and the relative data taken with the two sets of coils the absolute field for all the points was obtained. The deviations of these points from the average value are plotted in Fig. 32.

C. Betatron Acceleration Condition Measurements

The theoretical betatron condition which must be satisfied is $\dot{\phi}_o = 2\pi r_o^2 \dot{B}_o$ as previously noted. To achieve this condition the reluctance of the magnetic circuit in the flux bar path must be suitably altered so that each flux bar shunts the proper proportion of the flux down through the center of the orbit. This was done by shimming the flux bars out from the yoke slabs the proper amount as determined by visual examination of the betatron condition on a CRO.

A further adjustment of the position of the betatron period with respect to the zero field point was obtained by the use of a d.c. bias coil wound around the flux bars as shown in Fig. 34. The circuit used for examination of the betatron condition is shown in Fig. 35A. A typical CRO pattern obtained when the proper condition is satisfied is shown in Fig. 35B. The particular choice of the Furzehill CRO with direct coupled amplifiers was made to insure that the base line of the trace was the point of zero voltage across the input terminals. In RC coupled amplifiers this is not necessarily true because of the charging of the coupling capacitors. Another advantage of the Furzehill CRO is its ability to display without distortion a very small portion of the total vertical swing of the input signal. This is illustrated by the fact that Fig. 32

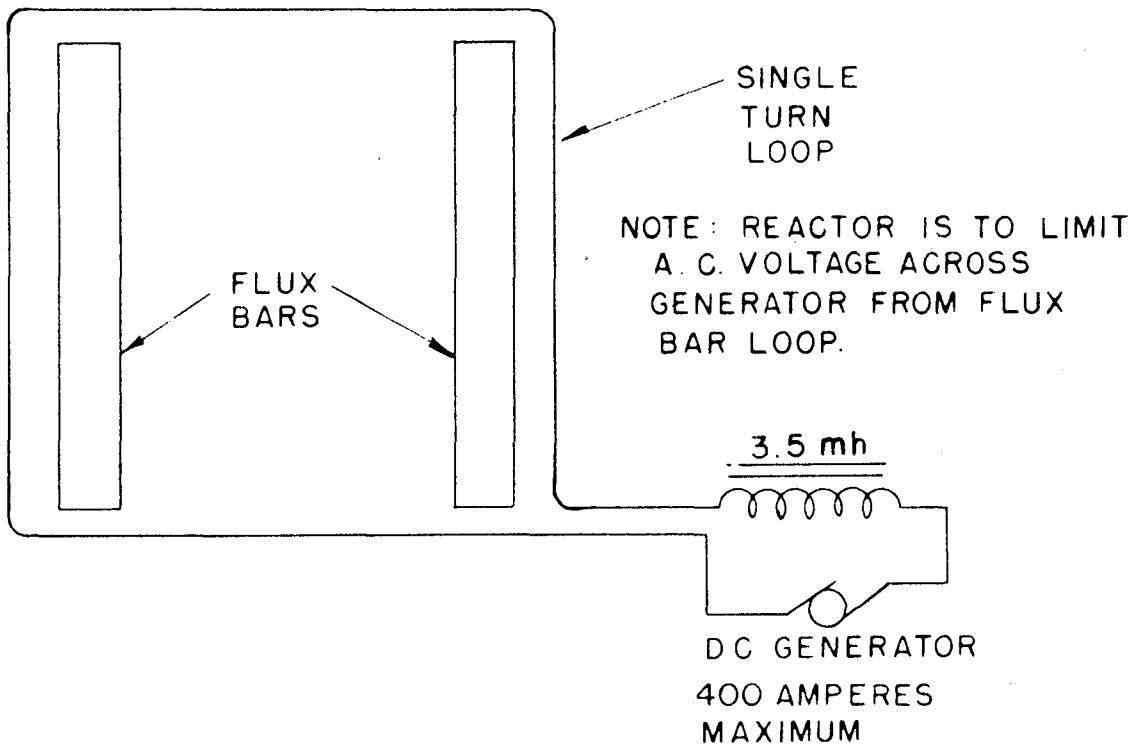

FLUX BAR BIAS CIRCUIT

FIG. 34

shows only about five percent of the input signal on the screen. In order to view the pattern on a triggered sweep an external sweep derived from the Du Mont Type 248 CRO was placed on the horizontal input terminals.

The orbit coil attenuator constant, as derived in Appendix D, is:

$$K = \frac{A_{sc}}{2\pi r_o^2} = \frac{1864.4}{2\pi \times 100^2} = .0302$$

where $r_o = 100$ cm

$$A_{sc} = 1864.4 \text{ cm}^2$$

This value was not in a convenient range for use with a General Radio Type 654A Decade Voltage Divider and further, the applied voltage of nearly 800 volts exceeded the rating of the Divider. To avoid these difficulties a carefully calibrated resistance of 90,000 ohms was inserted as shown in Fig. 35A. This made the Decade Box see one-tenth of the orbit coil voltage (the Decade Divider has a constant input impedance) and its new reading for the proper conditions was .302.

The procedure for determining the existing flux condition at any time was to move the search coil by ten inch increments around the track, adjust the attenuator until a pattern as shown in Fig. 35B was obtained, and record the attenuator setting. The flux acting on an orbital electron would be the average of these readings. Fig. 36 is a plot of the azimuthal variation. For each set of readings a flux bar adjustment was made. If the average setting was too high, the central flux was too low and the flux bars were moved closer to the yoke, thus decreasing the air gap. All the flux bar gaps were maintained equal except at the four corners where there were mechanical obstructions which made this impossible. The final gaps were .80 inches for the corner flux bars and .66 inches for the other fourteen flux bars.

The probable length of the betatron acceleration period was also investigated and found to be approximately fifty micro-seconds if a one percent variation of the betatron flux from the theoretical value is

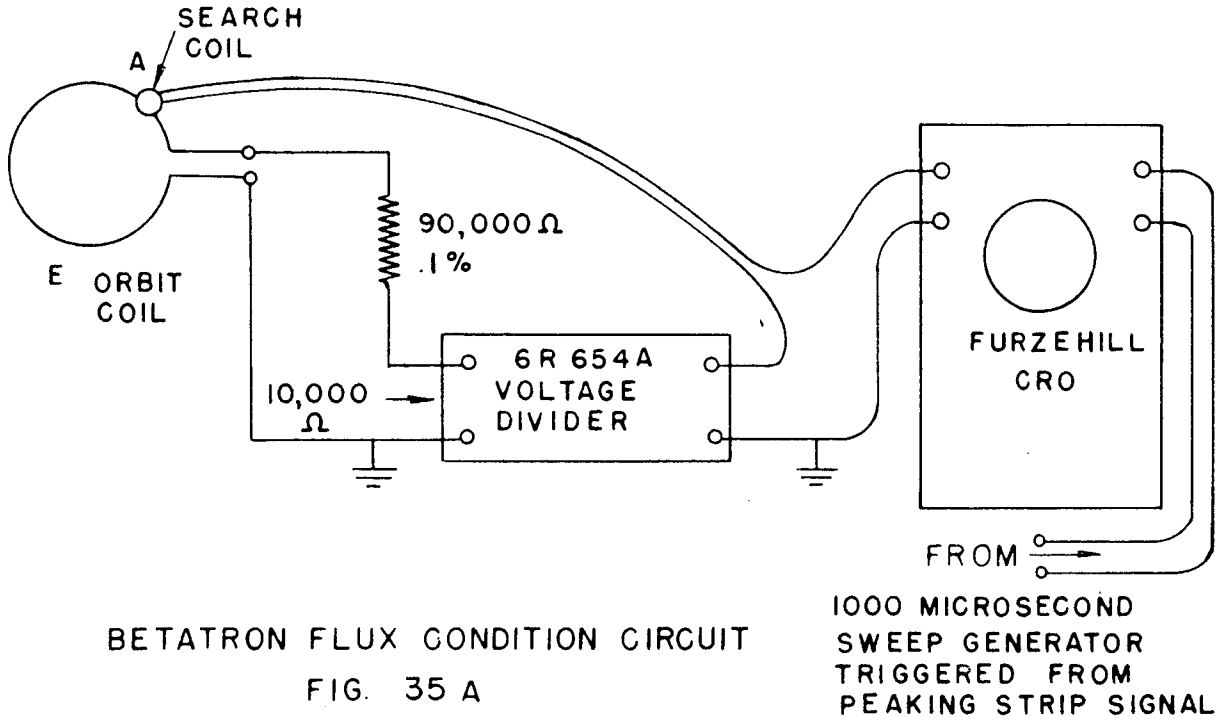

BETATRON FLUX CONDITION CIRCUIT

FIG. 35 A

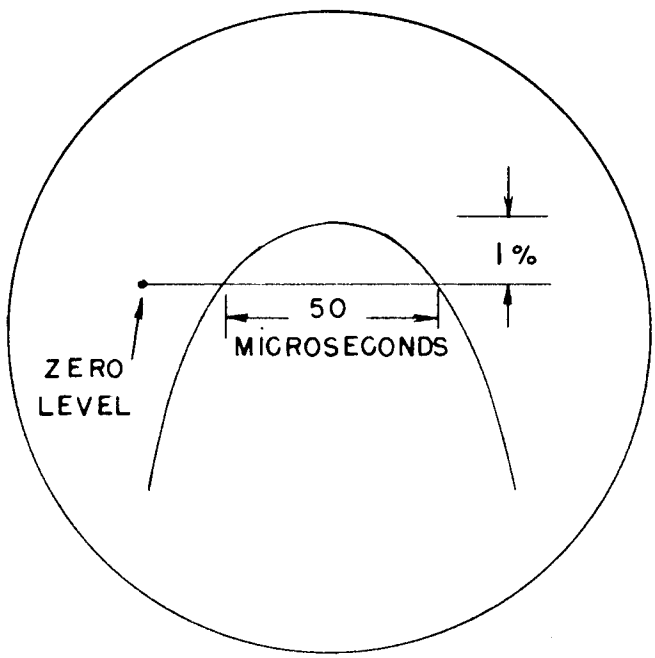

BETATRON FLUX MONITOR OSCILLOGRAM

FIG. 35 B

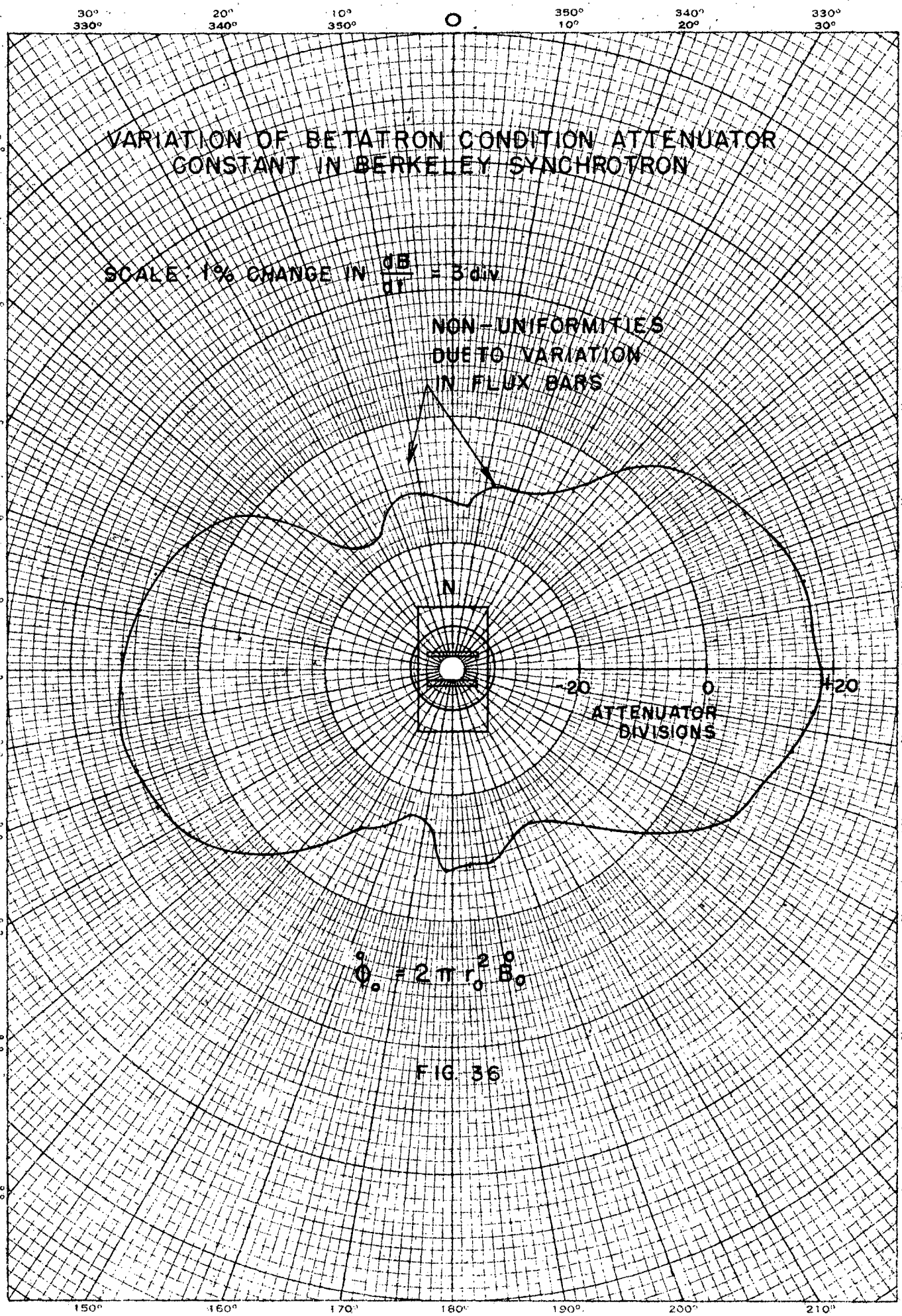

FIG. 36

allowed. This value was estimated on the basis of theoretical considerations as a reasonable value of allowed variation beyond which there was a good probability that the electrons would be thrown into the vacuum chamber walls. On the basis of later experience with the elctron beam this value was found to be more nearly three percent.

D. Phase Adjustments in the Azimuthal Magnetic Field

Two independent methods for adjustment of the azimuthal phase were provided in the magnet construction both employing the same basic principle which is elaborated in Appendix F. A coarse adjustment was obtained from a five turn coil wound around each separate slab in the North and South ends of the magnetic return path as shown on Fig. 2. Fig. 37 is a picture showing some of these coils. The terminals for each of these coils were brought out to separate variable resistances. As indicated in Appendix F if current is allowed to flow in such a coil the flux in its area of influence will be delayed by an amount proportional to the ampere turns of the coil. This allows an adjustment to be made by delaying all the slabs to the one with the greatest inherent lag.

A more refined adjustment of the phasing was obtained by the use of a series of radial wires, spaced one-half inch apart, and located between the pole base wedges and the pole face wedges as shown on Fig. 2. Both ends of each of these 1020 wires were brought to terminal boxes in such a manner that interconnections could be made to form correcting loops of nearly any desired area. In order to make the system more versatile a series of variacs, by means of which a voltage of either polarity could be applied to the radial wire compensating circuits, were connected as shown in Fig. 38. In order to conserve power, to attain greater adjustment range with small variac ratings and to increase the stability of operation these variacs were energized from the pulsed magnet excitation voltage. This was accomplished by placing two single turn loops around the magnet

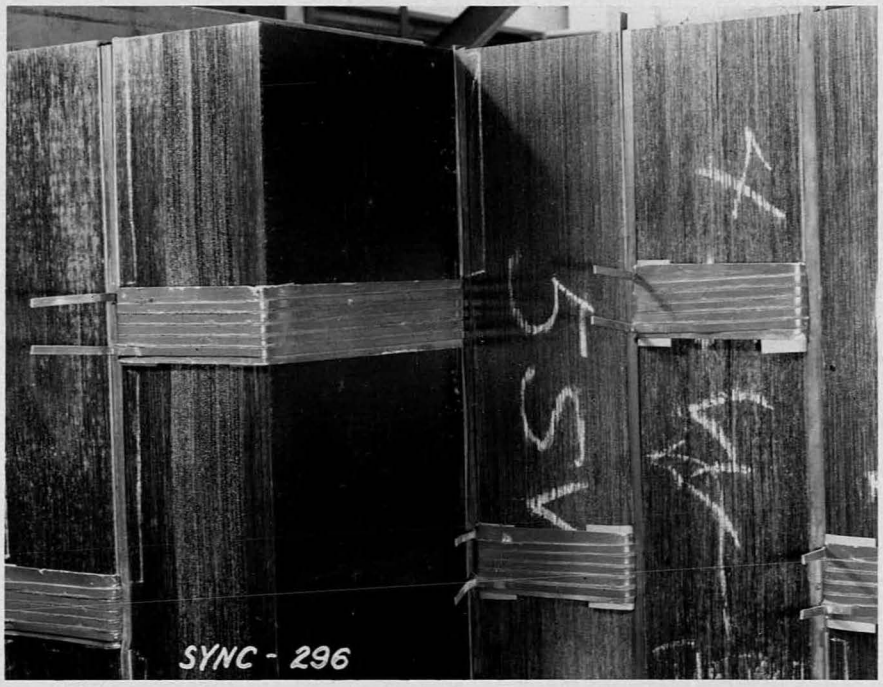

MAGNET YOKE EQUALIZING COILS

FIG. 37

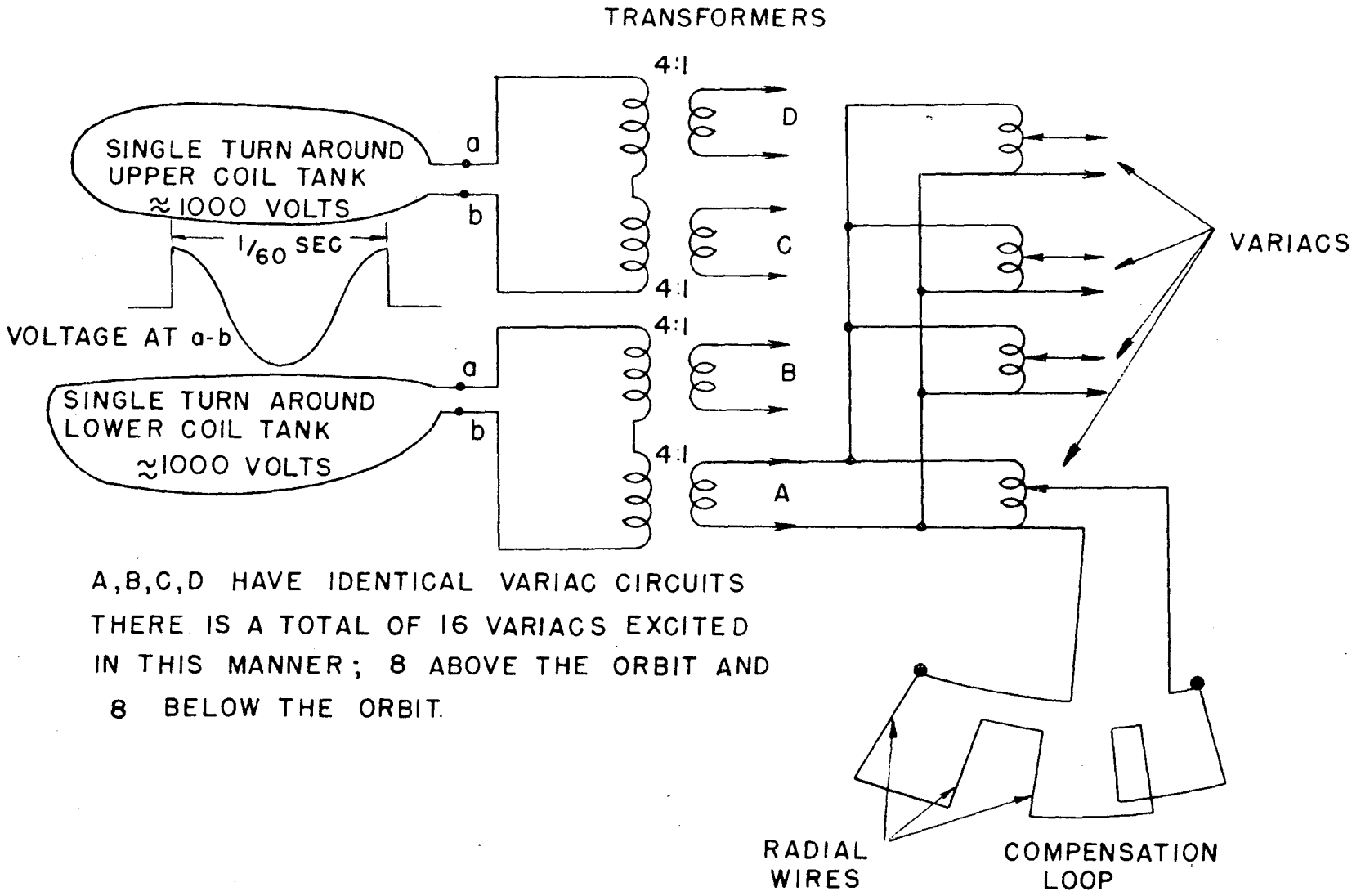

RADIAL WIRE EXCITATION CIRCUITS

FIG. 38

excitation coil tanks, one above the gap and one below the gap. These loops acted exactly as the secondary windings on a transformer and their output voltages were further transformed to a usable level and fed into the variacs as shown in Fig. 38. By adjusting the magnitude and polarity of the voltage output from the variacs the phasing may be adjusted over a wide range leading or lagging as required to obtain a "flat" (uniformly phased) field.

The measurements were made with a peaking strip mounted on the mobile ring with its output pulse presented on a synchroscope with a writing speed of four micro-seconds per inch. The synchroscope was triggered by a fixed peaking strip biased to trigger at a suitable time previous to the earliest zero field time in the magnet. The time between an arbitrary reference point on the sweep and the zero field time for one inch increments of azimuth was recorded, plotted as shown in Fig. 39A, and analyzed. On the basis of this analysis a new adjustment was made and the cycle repeated. The actual adjustment procedure proved to be fairly simple. The phase plot with no compensation is shown in Fig. 39A along with the plot for the final compensation. The initial step was to delay the North and South ends of the magnet in order to remove the obvious second harmonic. Then the fine adjustments were made with the radial wires. Identical adjustments were made in the radial wire circuits above and below the gap. A single variac was used to feed a complete quadrant of the magnet. The orbit is 255 inches in circumference and with a wire every one-half inch the total number of wires above the gap is 510. There are the same number below the gap. The total number of wires finally used was only a few percent of this as is seen in Fig. 40 which shows the actual connections in the magnet. Also shown on the diagram are the quadrant coils for variations in the second harmonic. The important field variation is that near the time of injection for at this time the variation is the largest percentage of the total field.

UNIVERSITY OF CALIFORNIA SYNCHROTRON
MAGNETIC FIELD ADJUSTMENT

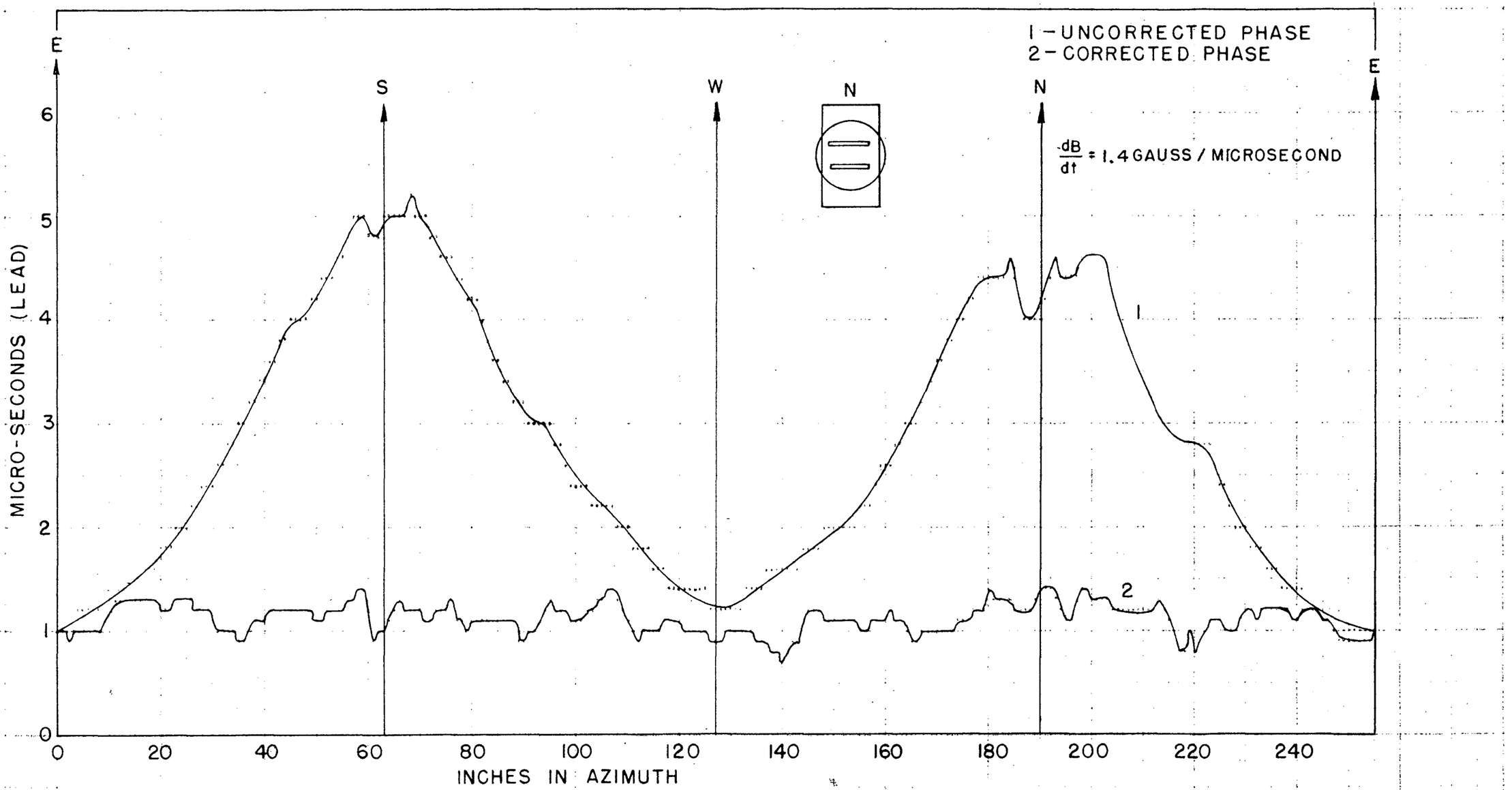

AZIMUTHAL PHASE PLOT (1ST HALF CYCLE OPERATION)

FIG. 39 A

13543-2

UNIVERSITY OF CALIFORNIA SYNCHROTRON
MAGNETIC FIELD ADJUSTMENT

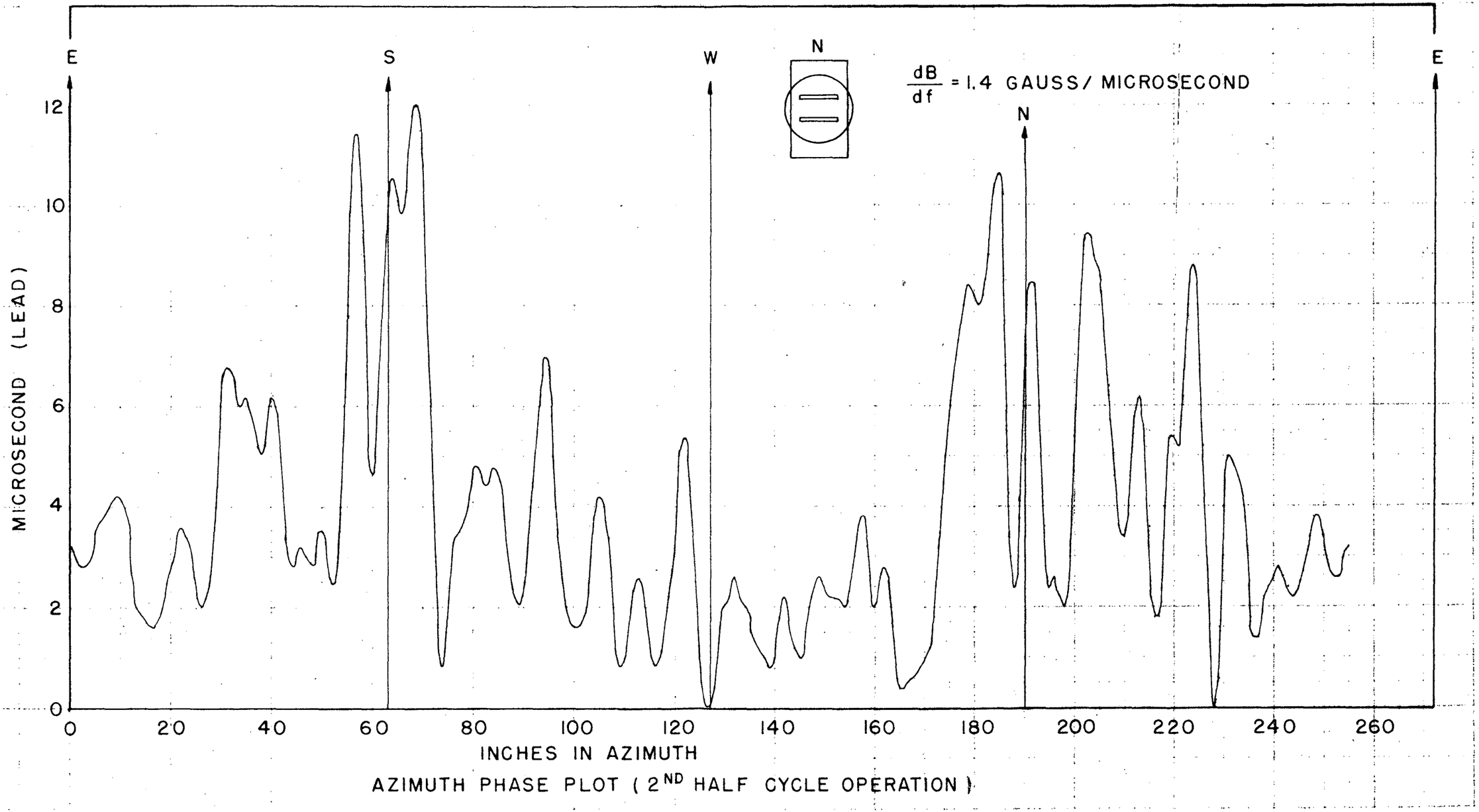

AZIMUTH PHASE PLOT (2ND HALF CYCLE OPERATION)

FIG. 39B

13711-1

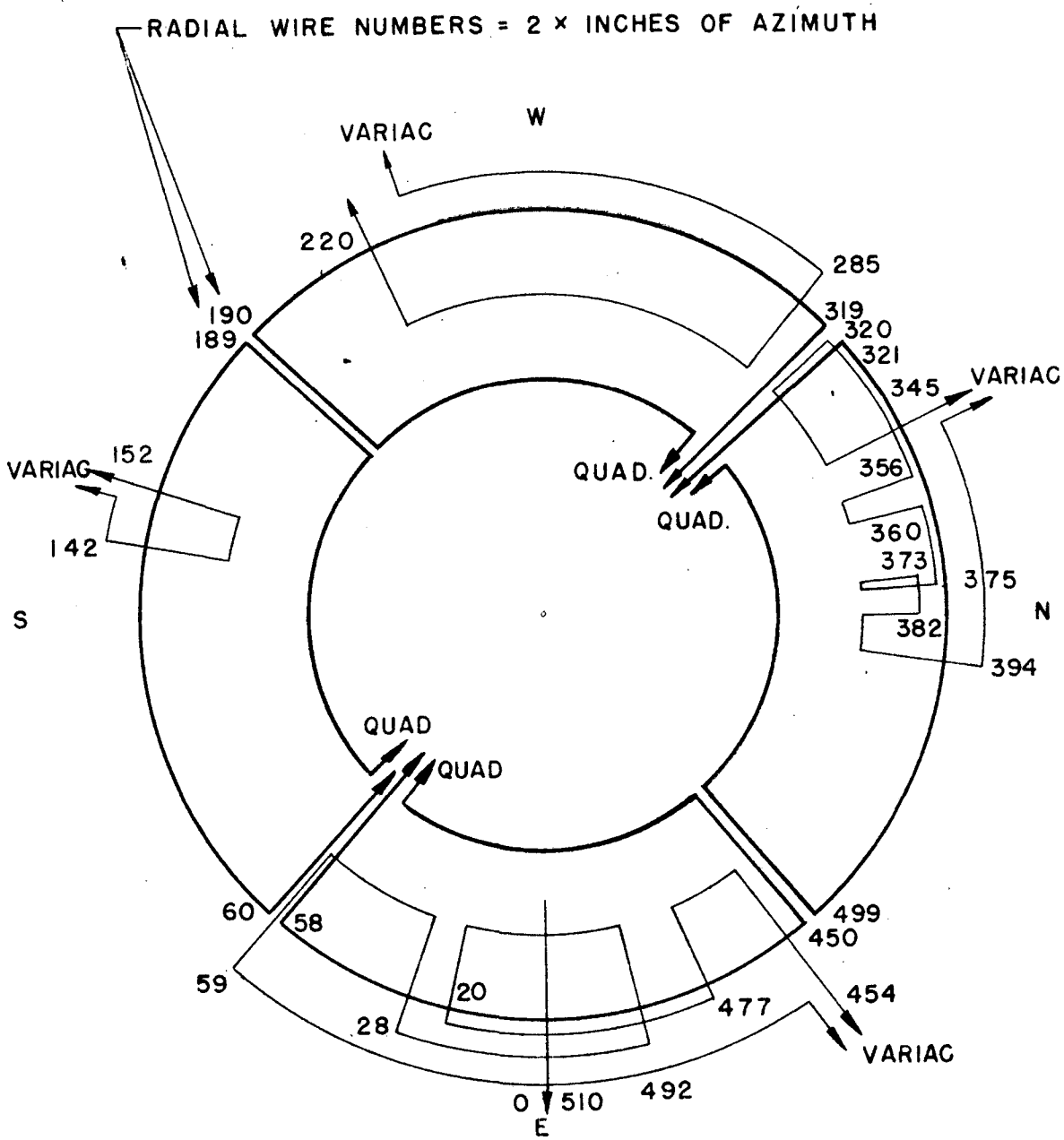

DIAGRAM OF RADIAL WIRE CORRECTIONS

FIG. 40

Investigation showed that the second harmonic component of the azimuthal field changed with peaking strip bias as a result of the difference in the rate of change of field between the north-south and east-west axes of the magnet as indicated in Fig. 36. For this reason the field was compensated at the predicted injection field of eight gauss. The quadrant coils were used as a vernier adjustment of the difference between actual and predicted injection points.

Because of the difficulties with starting transients it was found desirable to place a d-c magnetic bias field on the entire magnet so that the zero field point occurred about fifteen micro-seconds later than with the unbiassed condition. This required about 100 ampere-turns and was accomplished by using 8 turns around the outside of the excitation coil tank. The current was about 12 amperes for satisfactory operation.

Original designs called for operation on the second half cycle which would have avoided this difficulty but investigation revealed a remanence effect which increases the amplitude and number of phasing variations by an order of magnitude compared to the first half cycle operation. Figs. 39A and 39B show the phase plots for the two types of operation. It is interesting to note that it was only by chance that the rapid variations of Fig. 39B were identified as a remanence effect rather than an eddy current effect. At a time when only the north-half of the flux bars were installed a phase plot was made and found to have essentially the same pattern as for all the flux bars in place. If the effect were due to eddy currents there should have been less violent variations on the South side, where the flux bars were missing, because $\dot{\phi}$ in these slabs was less than $\dot{\phi}$ in the North side and eddy currents are proportional to $\dot{\phi}$ (or $\dot{B}$ as shown in Appendix A). This left only the possibility of remanence. To verify this the machine was operated at 30 cycles. If the effect were eddy currents all the variations should be the same as for 60 cycle operation

when expressed in terms of time as indicated in equation (3). However, if the effect were remanence the variations should be double their 60 cycle values as indicated by equation (6) because $\dot{\phi}_{60} = 2\dot{\phi}_{30}$ for a given $\dot{\phi}$ max. By this test the effect was definitely identified as remanence.

It is seen in Fig. 39A that the remanence variations are essentially zero. This is the result of the transient oscillation shown in Fig. 12A which demagnetizes the magnet. This oscillation is set up in a circuit consisting of the magnet inductance and the stray capacity of the excitation circuit. It is seen from Fig. 39A that the maximum excursion of the field after compensation is approximately .6 micro-second. It is obvious that the first three harmonics are of very small amplitude and above this value of ℓ in equation (1) the attenuation factor becomes so great that the summation is not seriously affected. It was not felt that the accuracy of the measurements or the labor involved justified a Fourier analysis.

CONCLUSION

It is important to note that the above adjustments were made on the basis of estimated requirements which were in every case as stringent as it was believed possible to achieve in practice. Little was known about the exact requirements of magnetic fields for this type of particle accelerator and the theory is vague about absolute criteria.

With this in mind it was not too surprising to find, after obtaining an electron beam accelerated for a number of revolutions, that the requirements are actually considerably less rigorous than our design requirements.

The final operating compensation consists simply of the radial wire circuits connected in eight equal portions above and below the orbit. Such an arrangement ofoctant coils allows control of the fundamental and lower harmonics. This is in agreement with Equation (1) which applies to first order effects. This first order theory for stable electron orbits appears to be adequate. It was believed that rapid variations in the azimuthal field might introduce second order perturbations in the orbits sufficiently large to be troublesome. In actual practice the machine was operated using the first quarter cycle and the third quarter cycle as accelerating periods. No appreciable difference in output was noted in spite of the fact that the 3rd quarter cycle has a large number of rapid variations with high amplitudes in the azimuthal field. The first order corrections were found to be extremely important and required a very high accuracy of adjustment.

In the early part of December, 1948, an electron beam of approximately 300 mev was obtained, and using a uranium target, gamma rays have been produced and detected by a number of different methods including zeus meters, photomultipliers, cloud chambers, and ionization chambers. Mesons have definitely been identified in nuclear plate exposures and many experi-

ments are possible at present. Much adjustment and development work on the operation of the machine will be necessary to achieve the optimum performance.

I would like to express my profound thanks to Dr. Wilson Powell, Dr. E. M. McMillan, Mr. Marvin Martin and the entire synchrotron staff for their private interest and suggestions. It was indeed a pleasure to work for and with such a group.

This work was performed under the auspices of the Atomic Energy Commission.

APPENDIX A

EDDY CURRENTS

In time varying magnetic circuits loss currents are set up within the iron due to its conductivity. Such a current can be expressed in terms of the rate of change of flux enclosed in a given loop. These loss currents can be limited by laminating the iron. Consider a single lamination as shown in Fig. 41. In order to simplify the calculation:

1. Assume $a \gg b$. This will invariably be the case for good design.
2. Neglect end effects by assuming the height of the lamination infinite. (Justification for this approximation will be made later.)
3. Assume uniform flux density over the x-y face of the lamination.
4. Assume that the flux enters along the z direction (normal to the x-y plane).

Faraday's induction law

$$\oint \mathcal{E} \cdot d\ell = -\frac{d}{dt}\int B \cdot n ds \qquad (32)$$

where $\mathcal{E}$ = electric gradient

B = magnetic induction

From (2) we can assume the electric gradient has only a y-component and is uniform. Very near the ends this would not be exactly true but in view of (1) they will contribute little to the total field. If we designate the electric gradient at some distance x from the origin as $\mathcal{E}_x$ and the total voltage around the circuit as E_x:

$$E_x = 2\int_{-a/2}^{a/2} \mathcal{E}_x \, dy$$

$$= \left[-\frac{d}{dt}\int_{-x}^{x} \int_{-a/2}^{a/2} B \, dydx \right]$$

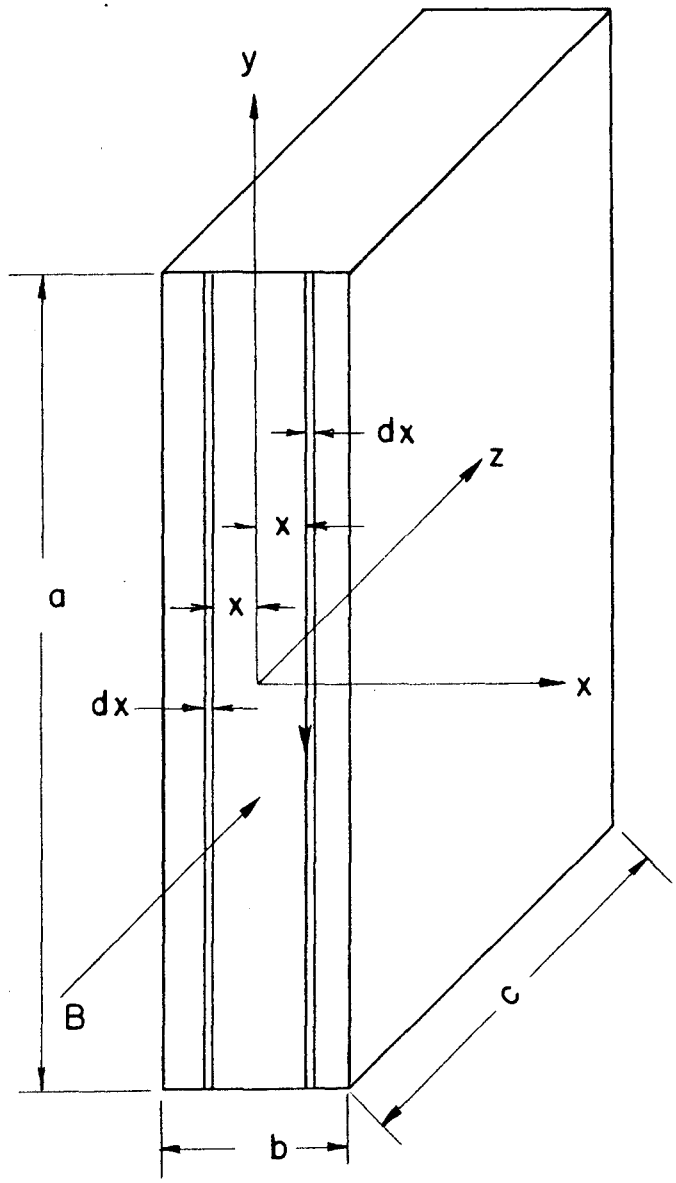

SAMPLE LAMINATION FOR
EDDY CURRENT ANALYSIS

FIG. 41

$$E_x = -\frac{d}{dt}\left[2axB\right]$$

$$= -2axB \times 10^{-8} \text{ volts}$$

The element of current, by ohms law, will be:

$$dI_x = \frac{E_x}{R_x}$$

$$R_x = \frac{\rho l}{dA} = \frac{\rho(2a)}{cdx} = \frac{2a\rho}{cdx}$$

$$dI_x = \frac{-2ax\dot{B}}{\frac{2a\rho}{cdx}} = -\frac{cxdx}{\rho}\dot{B} \times 10^{-8} \qquad (33)$$

where ρ = resistivity in ohm - cm

then:

$$I_x = \frac{-cx^2\dot{B}}{2\rho} \times 10^{-8} \text{ amperes} \qquad (34)$$

For $x = \frac{b}{2}$

$$I_{eddy} = -\frac{cb^2}{8\rho}\dot{B} \times 10^{-8}$$

$$= K\dot{B} \times 10^{-8} \text{ amperes} \qquad (35)$$

The field arising from the current dI_x will be:

$$dH_x = 4\pi(dI_x) = \frac{-4\pi cxdx}{10^9\rho} \qquad (36)$$

The average value of magnetic field intensity per centimeter of length of path will be:

$$H_{av} = \frac{\int_0^{b/2} A_x dH}{Ac} \quad \frac{-\int_0^{b/2} (2ax)(\dot{B})\left(\frac{4\pi cx}{10^9\rho}\right) dx}{abc}$$

$$= -\frac{\pi b^2\dot{B}}{3 \times 10^9\rho} \text{ oersteds} \qquad (37)$$

For a typical lamination in the synchrotron

$$b = .014 \text{ in.} = .0355 \text{ cm.}$$

$$\rho \approx 150 \times 10^{-6} \text{ ohm-cm.}$$

$$\dot{B} \approx 1.4 \times 10^6 \text{ gauss/sec.}$$

$$H_{av} = \frac{-\pi(.0355)^2\ 1.4 \times 10^6}{3 \times 150 \times 10^{-6} \times 10^9} \approx -.0123 \text{ oersteds/cm}$$

Eddy currents and their resultant out of phase fields are troublesome from a magnetic field standpoint only when they are not uniform throughout the magnetic structure. Non-uniformities cause phase variations. Such non-uniformities are due primarily to variable interlamination resistances which allow currents to flow from one lamination to another.

From a design standpoint eddy currents are important because they represent a power loss. If we use the power represented by Equation (33):

$$dP_x = 1/2(dI_x)^2_{max.} R_x$$

$$= 1/2\left[\left(\frac{\sigma^2 x^2 (dx)^2 (\dot{B}_{max})^2}{\rho^2}\right)\left(\frac{2a\rho}{\sigma dx}\right)\right]$$

$$= \frac{a\sigma x^2 dx}{\rho}(\dot{B}_{max})^2$$

Then the total power lost in a slab of thickness b is:

$$P_d = 2\int_0^{b/2} dP_x = \frac{a\sigma b^3}{12}(\dot{B}_{max})^2 \qquad (38)$$

Equation (38) shows clearly the importance of thin laminations to limit eddy current power losses.

APPENDIX B

MEASUREMENT OF THE MAGNETIC INDUCTION FIELD

A change in magnetic induction field can be measured by means of a search coil if the induced voltage in the coil is integrated. The induced voltage is:

$$E = -A \frac{dB}{dt} \times 10^{-8} \qquad (39)$$

E = induced e.m.f. in the coil.

A = effective area of the coil in $(cm.^2)$

B = magnetic induction in gauss.

If the field goes from an initial value B_1 at time t_1 to some final value B_2 at time t_2 then:

$$B_2 - B_1 = \frac{1}{A} \times 10^{+8} \int_{t_1}^{t_2} E(t)dt \qquad (40)$$

Then if we can obtain the integral of the e.m.f. from an electrical circuit the change in B can be measured. Such an integral can be obtained by using an RC integrator as shown in Fig. 42:

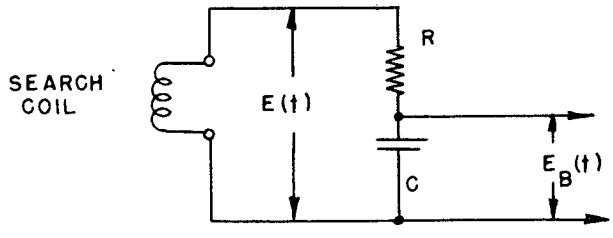

Fig. 42

INTEGRATOR

$$E(t) = iR + E_B(t) = R \frac{dQ}{dt} + \frac{Q}{C} \qquad (41)$$

Q = charge on capacitor C.

This is a differential equation with solutions of the form:

$$Q = ae^{-b(t_2-t_1)} + \frac{e^{-b(t_2-t_1)}}{R}\int_{t_1}^{t_2} e^{bt}\, E(t)dt \qquad (42)$$

Case I The Magnetic Field Variation.

E(t) is not of a form which lends itself to integration mathematically and further complications arise from the exponentials. We require a form:

$$E_B = \frac{Q}{C} = \frac{1}{RC}\int_0^t E(t)dt \qquad (43)$$

In order to approach (43) practically it is necessary to determine the constant $b = 1/RC$ in such a way that the exponential terms in (42) have a negligible effect during the period of time that we are interested in examining. This can be done by letting $\frac{t_2-t_1}{RC} \longrightarrow 0$. Assume $Q_o = 0$ at $t = t_1 = 0$. Then $a = o$ and (42) becomes:

$$Q = \frac{e^{-\frac{t_2}{RC}}}{R}\int_0^{t_2} e^{\left(\frac{t_2}{RC}\right)} E(t)dt \qquad (44)$$

The magnetic field goes through its cycle in $1/60 = .016$ seconds. Then if we set a limit of variation of 1 percent on the variation of the exponential term during this interval of time:

$$e^{-\frac{t_2}{RC}} = .99$$

$$-\frac{t_2}{RC} = \ln(.99) = -.01$$

$$RC \geq \frac{.016}{.01} = 1.6 \text{ seconds}$$

The second exponential, $e^{+\frac{t_2}{RC}}$ cannot be treated in so direct a manner since it is under the integral sign but by using the mean value theorem for integrals:

$$Q = \frac{e^{-\frac{t_2}{RC}}\, e^{\frac{t'}{RC}}}{R}\int_0^{t_2} E(t)dt = \frac{e^{-\frac{1}{RC}(t_2 - t')}}{R}\int_0^{t_2} E(t)dt \qquad (45)$$

where $0 < t' < t_2$

Then it can be said that the integration performed by a network with the constants evaluated above will always be better than indicated by the way they were derived because $t_2/RC > (t_2 - t')/RC$. Under these conditions:

$$E_B(t) \approx \frac{1}{RC}\int_0^{t_2} E(t)dt \tag{46}$$

Case II. A sinusoidal variation of E(t).

$$E(t) = E_0 \sin\omega t \tag{47}$$

Then in the steady state condition a solution of (41) is possible:

$$\begin{gathered} Q = Q_0 \sin(\omega t - \theta) \\ \tan\theta = RC\omega \\ Q_0 = \frac{E_0}{R\omega} \end{gathered} \tag{48}$$

Then $$E_v(t) = \frac{Q}{C} = \frac{E_0}{RC\omega}\sin(\omega t - \theta) \tag{49}$$

$$\text{for } RC\omega >> 1$$

$$E_v(t) \approx \frac{E_0}{RC\omega}\cos\omega t \tag{50}$$

Let $RC = 2$ and $\omega = 2\pi \times 60 = 377$, then $\tan\theta = 754$ and $\theta \approx 89^\circ 55'$ and the integration is exact to within 5 minutes of arc.

Field Calibration.

Eqs. (46) and (50) provide a means of calibrating the field change $B_2 - B_1$. If we present $E_B(t)$ from (46) on a CRO and set the vertical displacement from zero field to maximum field to some convenient amplitude then we can place a sinusiodal voltage $E_v(t)$ and adjust its amplitude to exactly the same value. Then we have:

$$\begin{gathered} E_B(t)_{max} = E_v(t)_{max} \\ \int_0^{t_2} E(t)dt = \frac{E_0}{\omega} \end{gathered} \tag{51}$$

in which E_0 can be measured accurately and ω is known.

Then from equation (40) $$B_2 - B_1 = \frac{E_0}{A\omega} \times 10^{+8} \tag{52}$$

where all the quantities on the right hand side are known and hence the difference in field is determined.

APPENDIX C

THE MEASUREMENT OF SMALL DIFFERENCES IN INDUCTION FIELD WITH SEARCH COILS

If there is a difference in the magnitude of the magnetic field at two points within a given time varying magnetic field region, it can be measured by bucking the outputs of two search coils located at different points in the field.

The resultant voltage obtained from two such coils will be the vector difference of the two separate voltages. Assuming the voltages to be very nearly in phase:

$$E = \left[A_1 B_1 - A_2 B_2\right] \frac{df(t)}{dt} \times 10^{-8} \qquad (53)$$

where: E = resultant voltage

ω = angular frequency of the magnetic field

B_1 = maximum field for coil #1

B_2 = maximum field for coil #2

A_1 = effective area of coil #1

A_2 = effective area of coil #2

$f(t)$ = magnetic field variation with time

Consider the conditions that exist in the actual test setup where A_1 is free to move in the field and A_2 is stationary at some reference point in the field. A_2 consists of two coils, A_3 fixed, and A_4 free to rotate about an axis perpendicular to the field. In general $A_3 + A_4 > A_1$. If θ is the angle of rotation of A_4 from its maximum effective area then:

$$E = \left[A_1 B_1 - B_2 \left(A_3 + A_4 \cos\theta\right)\right] \frac{df(t)}{dt} \times 10^{-8} \qquad (54)$$

$$= K \frac{df(t)}{dt} \times 10^{-8}$$

This can be integrated as set forth in Appendix B, in order to obtain a voltage E_B proportional to the change in field.

The most accurate adjustment which can be made with such a system is that for $E_B = 0$. For this case:

$$A_1 B_1 = B_2 (A_3 + A_4 \cos \theta) \tag{55}$$

If we denote the field at any general point, n, in the region by B_n and the angular rotation of A_1 which satisfies Eq. (55) by θ_n:

$$A_1 B_n = B_2 (A_3 + A_4 \cos \theta_n) \tag{56}$$

Consider the case where A_1 is at the same geometrical position as A_2, then $B_n = B_2$. Denoting this angle of rotation by θ_R:

$$A_1 = A_3 + A_4 \cos \theta_R \tag{57}$$

Substituting this into equation (55):

$$(A_3 + A_4 \cos\theta_R) B_n = B_2 (A_3 + A_4 \cos\theta_n) \tag{58}$$

$$\frac{B_n}{B_2} = \frac{A_3 + A_4 \cos \theta_n}{A_3 + A_4 \cos \theta_R} \tag{59}$$

The right hand side of this equation is completely determined for any position, n, and hence B_n is known as a ratio with B_2 and a relative field plot such as that shown in Fig. 32 is possible. This data can be obtained to a much higher degree of accuracy than is possible using a single coil. To illustrate compare the two cases. It is quite feasible to read a CRO trace to .05 inches. Using a single coil the maximum possible sensitivity would be about four inches for 10000 gauss. The possible error in this case is about 1.25 percent. Using the method outlined above, the sensitivity can be increased, using an external amplifier, to five gauss per inch. This corresponds to .0025 percent error. The discrepancy is not quite so great as this would indicate because there is also a fraction of a percent error in the reading of the angle.

APPENDIX D

THE ATTENUATOR CONSTANT FOR THE BETATRON ORBIT COIL

Given a single turn orbit coil and a search coil of effective electrical area A, it is desired to match the two voltages from these coils to determine the fullfilment of the betatron condition.

$$\dot{\phi} = 2\pi r_o^2 \dot{H}_o \tag{60}$$

$$N\dot{\phi} = E_{oc} \times 10^8 \tag{61}$$

$$A_{sc}\dot{H}_o = E_{sc} \times 10^8 \tag{62}$$

where: H_o = field intensity at the orbit

r_o = radius of the orbit

E_{oc} = orbit coil voltage

E_{sc} = search coil voltage

A_{sc} = effective electrical area of the search coil

N = one turn

then $$E_{oc} = \frac{2\pi r_o^2}{A_{sc}} E_{sc} \tag{63}$$

and $$K = \frac{E_{sc}}{E_{oc}} = \frac{A_{sc}}{2\pi r_o^2} = \text{attenuation ratio} \tag{64}$$

APPENDIX E

PEAKING STRIPS

Given a coil of N turns of wire wound around a strip of permalloy of cross-sectional area, A. If placed in a magnetic field with rate of change of flux, $\frac{d\phi}{dt}$, a voltage will be induced:

$$E = - N \frac{d\phi}{dt} \times 10^{-8} \qquad (65)$$

where E is the e.m.f. generated by changing flux in permalloy.

but $\phi = AB = A\mu H$

where B = magnetic induction in the permalloy

H = magnetic intensity in the permalloy

μ = permeability $\approx$ 50,000

Then

$$E = - N A\mu \frac{dH}{dt} \times 10^{-8} \qquad (66)$$

However, the permalloy saturates near H = .1 oersted and for all values of H greater than this the effective value of μ is 1. This means that E is present for a very short time while H goes from -.1 oersted to +.1 oersted as indicated in Fig. 43.

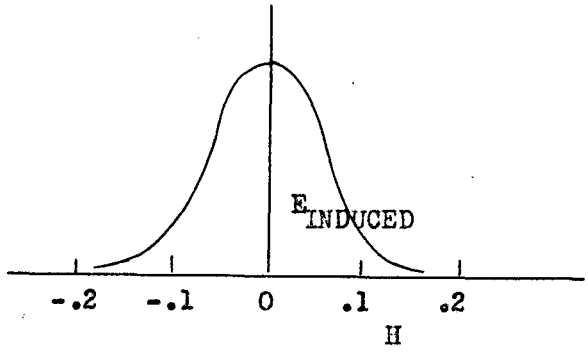

Fig. 43

IDEAL PEAKING STRIP VOLTAGE

Assuming $H = H_{max}\, f(t) = H_{max} \sin \omega t$ equation (66) becomes:

$$E = - N A \mu H_{max} \cos \omega t \times 10^{-8}$$

$$E_{max} = -N A \mu H_{max} \omega \times 10^{-8} \qquad (67)$$

N = number of turns on coil

A = area of permalloy

H_{max} = maximum magnetic intensity

$\omega = 2\pi f$ = angular frequency of field variation

μ = average permeability of permalloy

$\approx 50{,}000$ ($\mu_{max} = 100{,}000$)

APPENDIX F

ANALYSIS OF A LOOP AROUND A TIME VARYING FLUX

Examine a region throughout which there exists a time varying flux:

$$\phi_1 = \phi_{1\,max} \sin \omega t \tag{68}$$

If a coil of N turns is placed around this region as indicated in Fig. 44 a voltage E_1 will be induced:

$$E_1 = -N \frac{d}{dt} \times 10^{-8} \text{ volts}$$

$$= -N\phi_{1max}\omega \times 10^{-8} \cos \omega t$$

$$= K_1 \sin(\omega t + \frac{\pi}{2}) \tag{69}$$

If a resistance R is placed across the terminals of the coil, a current I_1 will flow and:

$$I_1 = \frac{E_1}{R} = \frac{K_1}{R} \sin(\omega t + \frac{\pi}{2}) \tag{70}$$

This current, I_1, will produce a flux ϕ_2 in the region enclosed and:

$$N\phi_2 = LI_1 \times 10^8 \tag{71}$$

$$\phi_2 = \frac{L}{NR} K_1 \cos \omega t \times 10^8$$

$$= \frac{-L\phi_{1\,max}\omega}{R} \cos \omega t \tag{72}$$

Then the total flux ϕ_t within the region is:

$$\phi_t = \phi_1 + \phi_2$$

$$= \phi_{1\,max}(\sin \omega t - \frac{\omega L}{R} \cos \omega t) \tag{73}$$

If a generator is added as shown in Fig. 45 with a voltage, E_g, proportional to E_1, a new current I_1' will flow:

$$I_1' = \frac{E_1 + E_g}{R}$$

$$E_g = K_2 E_1$$

$$I_1' = \frac{K_2 E_1 + E_1}{R} = \frac{E_1 (K_2 + 1)}{R} \tag{74}$$

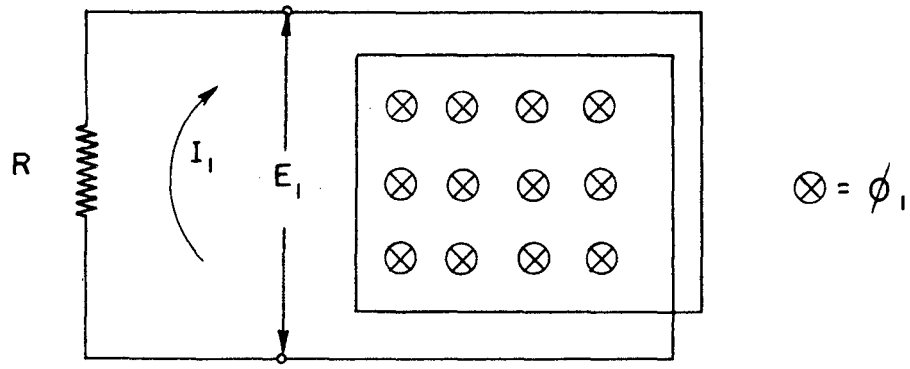

CONDUCTING LOOP ENCLOSING
A TIME VARYING FLUX

FIG. 44

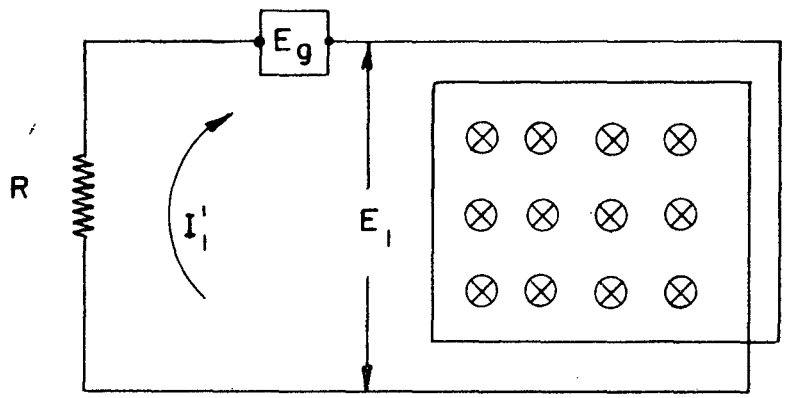

CONDUCTING LOOP WITH EXTERNAL
GENERATOR

FIG. 45

the constant K_2 depending on the polarity and magnitude of E_g.

If $K_2 > 0$ a phase lag is accomplished of greater magnitude than for the case where no generator is present. If $K_2 < 0$ the phase lag introduced by the current I_1 is opposed and if the magnitude of $E_g > E_1$ the phase in the region leads the phase it would have if no closed loop were present. In the actual case the induced voltage E_1 and the generator voltage E_g were not identical functions of time. This was not serious because the interval in which the adjustments were critical was only a few micro-seconds long and the curves were sufficiently matched during this time. The actual waveform for E_1 is shown in Fig. 12A and E_g is essentially a cosine function of the same fundamental frequency, 60 cycles.

BIBLIOGRAPHY

1. "The Synchrotron--A Proposed High Energy Particle Accelerator", E. M. McMillan, Phys. Rev., Vol. 68, Nos. 5 & 6, September 1945, pp. 143-144.

2. "The Theory of the Synchrotron", D. Bohm and L. Foldy, Phys. Rev., Vol. 70, Nos. 5 & 6, September 1946, pp. 249-258.

3. "The Stability of Electron Orbits in the Synchrotron", N. H. Frank, Phys. Rev., Vol. 70, Nos. 3 & 4, August 1946, pp. 177-183.

4. "Acceleration of Electrons by Magnetic Induction", D. W. Kerst, Phys. Rev., Vol. 58, No. 9, November 1, 1940, p. 841.

5. "Induction Electron Accelerator", D. W. Kerst, Phys. Rev., Vol. 59, No. 1, January 1, 1941, pp. 110-111.

6. "The Acceleration of Electrons by Magnetic Induction", D. W. Kerst, Phys. Rev., Vol. 60, No. 1, July 1, 1941, pp. 47-53.

7. "Electronic Orbits in the Induction Accelerator", D. W. Kerst and R. Serber, Phys. Rev., Vol. 60, No. 1, July 1, 1941, pp. 53-58.

8. "A Method for Measuring Small Changes in Alternating Magnetic Fields", Wilson M. Powell, Phys. Rev., Vol. 70, Nos. 5 & 6, September 1946, p. 444.

9. "Magnetic Fields Due to Dee Structures in a Synchrotron", Arnold F. Clark, Phys. Rev., Vol. 70, Nos. 5 & 6, September 1946, p. 444.

10. "Measurement of Out of Phase Magnetic Fields in the Betatron", W. Bosley, J. D. Craggs, D. H. McEwan, Nature (London), Vol. 159, No. 4033, February 15, 1947, p. 229.

11. "Magnetic Circuits and Transformers", E. E. Staff, M. I. T., John Wiley & Sons, Inc., 1943.